frontiers | Frontiers in Ecology and Evolution

TYPE Original Research
PUBLISHED 01 December 2022
DOI 10.3389/fevo.2022.1044565

OPEN ACCESS

EDITED BY
Wayne Iwan Lee Davies,
Umeå University, Sweden

REVIEWED BY
Dan-Eric Nilsson,
Lund University, Sweden
Lydia M. Mathger,
Marine Biological Laboratory (MBL), United States
Michael J. Pauers,
Milwaukee Public Museum, United States

*CORRESPONDENCE
Ronald H. Douglas
r.h.douglas@city.ac.uk

SPECIALTY SECTION
This article was submitted to Behavioral and Evolutionary Ecology, a section of the journal Frontiers in Ecology and Evolution

RECEIVED 14 September 2022
ACCEPTED 07 November 2022
PUBLISHED 01 December 2022

CITATION
Wagner H-J, Genner MJ, Partridge JC, Chung W-S, Marshall NJ, Robison BH and Douglas RH (2022) Diversity and evolution of optically complex eyes in a family of deep-sea fish: Ocular diverticula in barreleye spookfish (Opisthoproctidae). *Front. Ecol. Evol.* 10:1044565. doi: 10.3389/fevo.2022.1044565

Diversity and evolution of optically complex eyes in a family of deep-sea fish: Ocular diverticula in barreleye spookfish (Opisthoproctidae)

Hans-Joachim Wagner[1], Martin J. Genner[2], Julian C. Partridge[3], Wen-Sung Chung[4], N. Justin Marshall[4], Bruce H. Robison[5] and Ronald H. Douglas[6]*

[1]Anatomisches Institut, Universität Tübingen, Tübingen, Germany, [2]School of Biological Sciences, University of Bristol, Bristol, United Kingdom, [3]UWA Oceans Institute, The University of Western Australia, Perth, WA, Australia, [4]Queensland Brain Institute, University of Queensland, Brisbane, QLD, Australia, [5]Monterey Bay Aquarium Research Institute, Moss Landing, CA, United States, [6]Division of Optometry and Visual Science, City, University of London, London, United Kingdom

Several families of mesopelagic fish have tubular eyes that are usually upwardly directed. These maximise sensitivity to dim downwelling sunlight and dorsal bioluminescence, as well as facilitating the detection of dark silhouettes above the animal. Such eyes, however, have a much-reduced field of view and will not be sensitive to, for example, lateral and ventral bioluminescent stimuli. All mesopelagic Opisthoproctidae so far examined have evolved mechanisms for extending the limited visual field of their eyes using approximately ventrolaterally directed, light-sensitive, diverticula. Some genera have small rudimentary lateral retinal areas capable of detecting only unfocussed illumination. Others have more extensive structures resulting in eyes that simultaneously focus light from above onto the main retina of the tubular eye using a lens, while diverticula produce focussed images of ventrolateral illumination using either reflection or possibly refraction. These bipartite structures represent perhaps the most optically complex of all vertebrate eyes. Here we extend the limited previous data on the ocular morphology of five Opisthoproctidae (*Opisthoproctus soleatus*, *Winteria telescopa*, *Dolichopteryx longipes*, *Rhynchohyalus natalensis, and Bathylychnops exilis)* using a combination of histology and magnetic resonance imaging and provide a preliminary description of the eyes of *Macropinna microstoma*. We note an increase in diverticular complexity over the life span of some species and quantify the contribution of the diverticulum to the eye's total neural output in *D. longipes* and *R. natalensis* (25 and 20%, respectively). To help understand the evolution of Opisthoproctidae ocular diversity, a phylogeny, including all the species whose eye types are known,

was reconstructed using DNA sequences from 15 mitochondrial and four nuclear genes. Mapping the different types of diverticula onto this phylogeny suggests a process of repeated evolution of complex ocular morphology from more rudimentary diverticula.

KEYWORDS

tube eye, diverticulum, visual field, Opisthoproctidae, phylogeny, eye evolution, barreleye

Introduction

Although most mesopelagic fish have conventional, approximately spherical, laterally positioned, eyes (Locket, 1977; Wagner et al., 1998), members of several genera have evolved usually upwardly directed, elongated, tube-shaped eyes (Brauer, 1908; Contino, 1939; Munk, 1966; Locket, 1977; Collin et al., 1997; **Supplementary Material 1** for further details) as an adaptation to the directional nature of light in the deep ocean. A well-developed main retina lines the base of such tubular eyes and receives focussed illumination *via* an approximately spherical lens. This morphology serves primarily to maximise sensitivity to a necessarily limited part of the visual field usually encompassing the relatively brighter, but nonetheless dim, downwelling sunlight. This allows the detection of silhouettes of dark objects higher in the water column and the detection of bioluminescence above the animal.

In general, absolute visual sensitivity is increased by a large pupil, which usually requires a large eye (Land and Nilsson, 2012; de Busserolles et al., 2013; Nilsson et al., 2014). As most mesopelagic fish are relatively small, there is an upper limit to the eye size they can accommodate. However, as tubular eyes correspond to the central portion of normal spherical eyes that have been peripherally reduced (Franz, 1907; Locket, 1977), they allow small animals to have eyes with relatively large pupils and lenses, and hence enhanced sensitivity without the space requirements and metabolic costs of larger eyes (Johnsen and Haddock, 2022). The binocular overlap afforded by such eyes will further increase absolute sensitivity to downwelling light (Weale, 1955) and may also provide a cue for determining object distance (Brauer, 1902).

Nevertheless, such tubular eyes have a significant functional disadvantage as their main retina has a very restricted, roughly cone-shaped, visual field with an apex plane angle of only approximately 50^{o} (corresponding to a solid angle of ca. 0.6 sr) directly above the animal (**Supplementary Figure 1**; Warrant and Locket, 2004). Consequently, such eyes will not detect animals or their diverse bioluminescent emissions (Herring, 1990; Widder, 1999; Haddock et al., 2010) outside of their limited field of view. A rudimentary accessory retina lines the medial wall of most tubular eyes and will increase their visual field laterally by around 70° beyond that provided by the main retina (Warrant and Locket, 2004; **Supplementary Figure 1**). However, it receives only unfocussed light and will thus lack the sensitivity provided by a focussed image. Furthermore, the total visual field of the eye will still be deficient lateroventrally. Not surprisingly therefore, animals with tubular eyes show a variety of adaptations to overcome their otherwise restricted visual field.

At least one species, *Macropinna microstoma* is capable of extensive eye movements (Robison and Reisenbichler, 2008), enlarging its field of view by scanning the environment. It is also possible that a similar function could be achieved by reorientation of the body or head. However, even with eye or body movements, tubular eyes will still have only a limited visual field at any one time. It is therefore perhaps not unexpected, that some mesopelagic fish have evolved adaptations to permanently enlarge the visual fields of their tubular eyes. The scopelarchids (Brauer, 1908; Munk, 1966; Locket, 1971, 1977; Collin et al., 1998) and evermannelids (Locket, 1977; Wagner et al., 2019), for example, possess 'lens-pads' and 'optical folds,' respectively, below their corneas which are presumed to be optical structures that direct ventrolateral illumination into the dorsally directed tubular eyes. More commonly, other genera have small areas of well-developed retina within diverticula on the lateral wall of their tube eyes, which light reaches through ventrolaterally directed transparent 'windows.'

Diverticula such as these are common in the Opisthoproctidae (aka barreleyes or spook fish), a remarkable family of argentiniform teleosts that inhabit lower mesopelagic and bathypelagic depths (*ca.* 400–2,500 m) and incorporate some of the most exotic looking deep-sea fish. These include, the triangular prism-shaped *Opisthoproctus* sp. whose large flattened ventral 'soles' can be hidden from observers lower in the water column by bioluminescent secretions from a modified part of the intestinal tract (Denton et al., 1985; Poulsen et al., 2016), the 'four-eyed' *Bathylychnops exilis* (Pearcy et al., 1965), and 'the alien looking' *M. microstoma* whose 'green' tubular

Abbreviations: MRI, magnetic resonance imaging; PBS, phosphate buffered saline; Gd-DTPA, N-methylglucamine salt of the gadolinium complex of diethylenetriamine pentaacetic acid; SL, standard length; RI, refractive index; ar, accessory retina; ce, ciliary epithelium; cp, corneal projection; d, diverticulum; Chor, inner choroid; GCL, ganglion cell layer; INL, inner nuclear layer; IPL, inner plexiform layer; mr, main retina; OLM, outer limiting membrane; ONL, outer nuclear layer; OPL, outer plexiform layer; ros, rod outer segments; RPE, retinal pigment epithelium; Sc, sclera; sl, scleral lens; c, caudal; d, dorsal; l, lateral; m, medial; r, rostral; v, ventral.

eyes are embedded in a dome shaped gelatinous protective shield (Robison and Reisenbichler, 2008; Johnsen and Haddock, 2022). The structure and optics of the diverticula within this family are particularly diverse. Like species in other families with tube-eyes (*e.g., Stylephorus chordates, Gigantura* sp.), some Opisthoproctidae have relatively simple, afocal, light-detecting diverticula (Brauer, 1908; Bertelsen et al., 1965; Munk, 1966; Frederiksen, 1973; Locket, 1977; Collin et al., 1997), while others have more extensive diverticula potentially capable of image formation (Pearcy et al., 1965; Wagner et al., 2009; Partridge et al., 2014).

Mesopelagic fish are not rare, and in fact they include some of the most abundant vertebrate species on the planet. Due to the low density of animals in the deep-sea, however, and the limited opportunity to sample them, these animals are rarely caught. Thus, descriptions of the ocular structure of entire species of deep-sea fish often rest on a very low number of individuals, sometimes only a single eye that furthermore could have been damaged during capture or, especially in museum specimens, have artefacts attributable to tissue fixation. This, and the fact that ocular structure of fish can change significantly with age, has limited the significance of the available data.

Here we re-examine aspects of the eyes of five species of Opisthoproctidae whose ocular structure has previously been described (*Opisthoproctus soleatus*, *Winteria telescopa*, *Dolichopteryx longipes, Rhynchohyalus natalensis, and B. exilis*) to highlight any inter-individual variation including ontogenetic differences. In *D. longipes* and *R. natalensis* we also assess the relative importance of the diverticulum by determining the total neuronal output of both the diverticulum and the main retina. We also give an initial outline of the structure of the eye of another opisthoproctid, *M. microstoma*, which has not been described before in detail, although a preliminary description has been given (Frederiksen, 1973).

The bipartite eyes of *D. longipes, R. natalensis,* and *B. exilis*, which simultaneously focus downwelling illumination *via* a lens within a main eye, and ventrolateral light using diverticula that potentially produce focused images using either reflection or refraction, represent arguably the most optically complex eyes of all vertebrates. How they might have evolved is therefore of interest. To this end it would be useful to map the known ocular structure of the Opisthoproctidae onto a robust phylogeny.

Due to the relative infrequency with which some opisthoproctid species are caught, and their relative fragility, they are scarce in collections. Nevertheless, over recent years our understanding of their taxonomic diversity and phylogenetic relationships has improved (Parin et al., 2009; Poulsen et al., 2016; Prokofiev, 2020). The 10 currently recognised genera are split into two broad categories based on the number of vertebrae (Prokofiev, 2020): short-bodied (30–40 vertebrae; *Monacoa*, *Opisthoproctus*, *Winteria*, *Macropinna*, and *Rhynchohyalus*) and long-bodied (40–85 vertebrae; *Dolichopteryx, Dolichopteroides*, *Ioichthys*, *Bathylychnops*, and *Duolentops*), and currently comprise 23 valid species (Fricke et al., 2021). Two genera of short-bodied opisthoproctids (*Monacoa* and *Opisthoproctus*) are referred to as 'sole-bearing' based on their characteristic flattened ventral surface (**Figure 1a**).

Unfortunately, the most comprehensive phylogeny of this family (Poulsen et al., 2016) is incomplete and does not include some of the species known to have diverticula. We therefore constructed a more extensive phylogeny for the Opisthoproctidae, including all the species whose ocular morphology is known, using available mitochondrial and nuclear DNA sequences in order to examine potential evolutionary pathways for their complex ocular diversity.

Materials and methods

Animals

Four of the species examined here (*O. soleatus*, *W. telescopa*, *B. exilis*, and *M. microstoma*) were caught specifically for this study, while *D. longipes* and *R. natalensis* were captured as part of previous work (Wagner et al., 2009; Partridge et al., 2014). All animals were caught using rectangular midwater trawls at various locations and depths during multiple deep-sea expeditions. Basic morphometric data and details of animal capture are given for all animals examined in **Table 1**.

Most eyes were fixed immediately following capture in 4% paraformaldehyde and 2.5% glutaraldehyde. However, those of *R. natalensis* were fixed in 70% ethanol and formalin, while the eyes of *M. microstoma* were preserved in 10% paraformaldehyde and ethanol.

Our specimens were examined using conventional histology and/or magnetic resonance imaging (MRI), both of which are subject to artifacts caused by, for example, tissue shrinkage. Protocols were employed that minimised such problems. While histological sectioning allows details of cellular organisation to be seen in two dimensions, MRI provides spatial information of internal anatomy and excellent contrast in soft tissue. The 3D rendering of eyes using MRI also provides digitised visualisation allowing examination from different angles and the determination of the best sectioning angle for histology.

Histology

Due to the different sizes and fixation protocols, individual approaches were used to obtain serial sections for each eye that would allow a 3D reconstruction of the entire eye or parts of it, but at the same time, enable the study of structures of special interest at the ultrastructural level. Thus, all isolated eyes were postfixed in 2.5% phosphate-buffered glutaraldehyde, dehydrated, and embedded in Epon 812 (Serva, Heidelberg, Germany). To facilitate impregnation, the cornea and lens of

TABLE 1 Animals used in this study.

Species	SL (mm)	Max rec SL (mm)	Eye height (mm)	Eye width (mm)	Lens diam (mm)	Capture depth (m)	Location	Ship/Cruise id	Use	Figure
Opisthoproctus soleatus (Vaillant, 1888)	42	105	7.2	5.1	3.8	500–700	North Atlantic	RRS Discovery 243	Histology	Figure 1
Winteria telescopa (Brauer, 1901)	42	150	5.9	3.9	2.8	600–800	Indian Ocean	FS Sonne 258-1	Histology MRI	Figure 2
Dolichopteryx longipes (Vaillant, 1888)	102	180	6.8	4.1	3.9	600–800	South Pacific	FS Sonne 194	Histology	Figures 3, 4 and Supplementary Figure 2
	93		5.2	3.1	2.9	600–800	Indian Ocean	FS Sonne 258-1	MRI	
	52		3.1	2.0	2.0	600–800	Indian Ocean	FS Sonne 258-1	MRI	
Bathylychnops exilis (Cohen, 1958)	200	580	7.5	9.2	4.5	400–600	North Atlantic	RRS Discovery 243	Histology	Figures 5, 6
Macropinna microstoma (Chapman, 1939)	32	150	3.9	2.9	2.6	637	Eastern Pacific	RV Western Flyer, 489	Histology	Figures 7, 8
	55		8.4	7.7	4.7	600–800	Eastern Pacific	RV Western Flyer, 2784	Histology MRI	
Rhynchohyalus natalensis (Gilchrist and von Bonde, 1924)	183	160	33.9	26.5	13.9	800–1000	South Tasman Sea	RV Southern Surveyor	Histology MRI	Supplementary Figure 3

Standard length, eye height and width were, where available, measured in fresh unfixed material. The dimensions measured from the MRI scans or histological sections shown in this manuscript may differ slightly from the values shown in the table due to both shrinkage during fixation as well as the plane of sectioning/scanning which was usually chosen to best represent the diverticula rather than show maximum ocular dimensions. Lens diameter, which is less affected by fixation, was determined after enucleation or from histological sections. The maximum recorded size for a species is taken from Fishbase (Froese and Pauly, 2021).

10.3389/fevo.2022.1044565

10.3389/fevo.2022.1044565

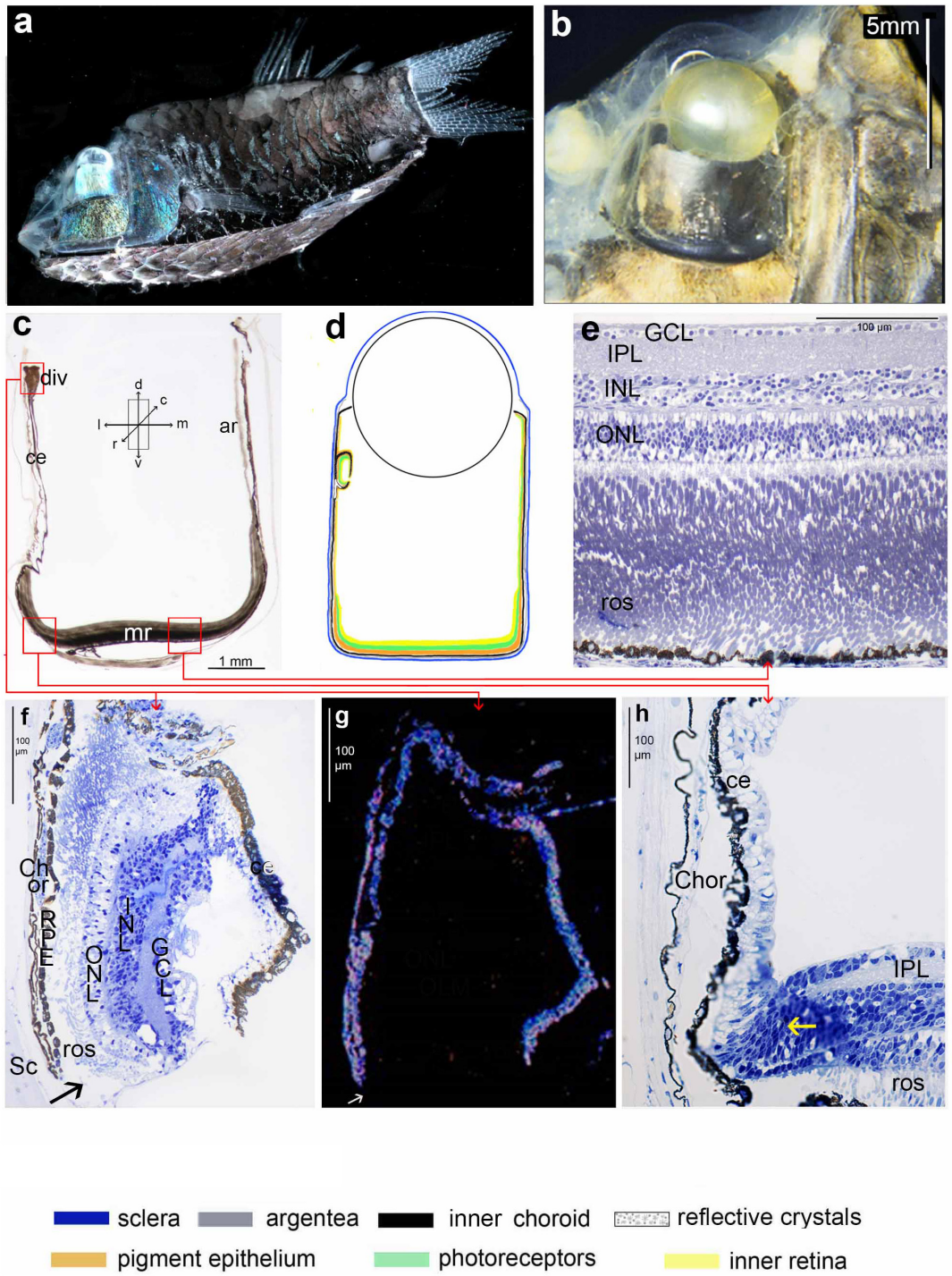

FIGURE 1
Opisthoproctus soleatus: **(a)** side view of an entire animal (SL 42 mm) showing the tubular eye and the flattened sole plate on the ventral surface of the animal (courtesy E. Widder); **(b)** head of another individual used for histology in this study (SL 42 mm); **(c)** approximately transverse thick section of tube eye with lens removed: note the well-developed main retina on the base of the tube, the accessory retina on the medial wall and the ciliary epithelium on lateral wall with a diverticulum dorsally; **(d)** schematic diagram of ocular layers; the colour code listed at the bottom of the figure applies to this and subsequent diagrams; **(e)** radial semithin section of the main retina; **(f)** radial semithin section of diverticulum. The ventral arrow indicates the point of entry of light through an unpigmented region of the lateral wall of the diverticulum; **(g)** same section as f seen in dark-field illumination highlighting reflective structures in the choroid and pigment epithelium; **(h)** radial semithin section of the transition of the main retina to the lateral wall, the yellow arrow indicates the cell proliferation zone. The approximate orientation relative to the body axis of panels **(c–h)** is indicated by the arrows shown in the inset of panel **(c)** but see Materials and Methods for comments on deviations from the transverse plane in histological sections.

the (main) tube eye were removed in larger specimens. As the orientation of the tubular eyes is variable, blocks containing the enucleated eyes were oriented so that sections were produced parallel to the long axis of the eye, irrespective of how the eye was positioned in the fish, and perpendicular to the diverticulum centre. Initially, serial sections were cut at a thickness of 2μm in the case of *D. longipes*; subsequently, all other eyes were sectioned at 25μm and mounted on plastic slides. As a rule, every fifth section (or tenth section in *R. natalensis* being the largest specimen) was photographed on a Zeiss stereomicroscope and used for 3D representation of the eye; in areas of special interest, each section was recorded. Selected sections were re-sectioned to produce 1 or 2μm thick semithin sections. Some of the thick and thin sections were stained with a mixture of methylene blue and Azur II (Richardson et al., 1960). They also served as material for cutting ultrathin sections. To test the reflective nature of structures some sections were examined in a combination of dark-field and polarised illumination (see Wagner et al., 2009 for details). Light and electron micrographs (Zeiss/LEO EM912) were recorded digitally.

In both histological sections and MRI scans (see below), we define 'transverse' sections/scans as those taken approximately perpendicular to the long axis of the body. 'Sagittal' and 'horizontal' are parallel to the long axis, with 'sagittal' in the dorsoventral, and 'horizontal' in the mediolateral plane. As sections were always cut perpendicular to the centre of the diverticulum, in the two species where the diverticulum is lateral (*D. longipes* and *R. natalensis*) eyes were sectioned in a transverse plane. However, in three species (*O. soleatus*, *B. exilis*, and *M. microstoma*) the diverticulum is more rostrolateral and in another (*W. telescopa*) ventrolateral. In these animals the cutting of sections perpendicular to diverticulum will result in a plane of sectioning not quite parallel to any of the main body axes. Nonetheless, in an attempt to make the descriptions more easily comparable between the species, in the case of the four latter species the text and the orientation arrows in the figures (**Figures 1**, **2**, **5**–**8**) indicate the major orientation axes, even though the histological sections deviate somewhat from these orientations.

A further complicating factor is that in some of these species the position of the eyes is not fixed within the head and they are capable of at least some rotation in the vertical plane. Unless indicated otherwise the orientation of various ocular structures is described using the ocular orientation usually observed in freshly caught specimens; dorsal in all species except for the rostrally directed eyes of *W. telescopa*.

In both eyes of a single *R. natalensis* and in one eye of *D. longipes* (SL 102 mm), the surface areas of the diverticular retina and the main retina lining the base of the tubular eye were calculated. In these eyes, the number of axons in the optic nerve and the fascicle made up of retinal ganglion cells exiting the diverticulum were estimated by counting the number of axons in ultrathin electron microscopic sections from areas distributed at random across the surface of the structures and covering at least 20% of their total area. Optic nerve counts were made in sections cut between the exit from the eye and the optic chiasm, while axons in the diverticular fascicle were quantified at the level of the septum between the main eye and the diverticulum. The total number of axons exiting the diverticula and main retina was estimated by assuming the same density throughout the entire structure as in the counted sections. Thus, the retinal ganglion cell densities calculated represent an average density, rather than the maximum density usually used to calculate optimal spatial resolution.

These observations were augmented by external examination of specimens kept in the Spirit Collection of the Natural History Museum, London and the Discovery Collections at the National Oceanography Centre, Southampton.

Magnetic resonance imaging

Specimens were removed from the storage medium and repeatedly rinsed with 0.1 M PBS to minimise fixative residue. The rehydrated specimens were then soaked in 0.1 M PBS containing MRI contrast agent, 0.2% ionic Gd-DTPA (Magnevist) (Bayer, Leverkusen, Germany), for 24–48 h to enhance image contrast prior to MRI. These contrast-enhanced samples were imaged following the protocol developed by Partridge et al. (2014) with additional modification. The contrast-enhanced specimen was put into a fomblin-filled (Fomblin oil, Y06/6 grade, Solvay, United States) container to prevent dehydration and placed in a vacuum chamber for 3 min to remove air bubbles trapped inside the orbit or soft tissue. The container was then placed in a custom-built 20 mm diameter surface acoustic wave coil (M2M Imaging, Brisbane, Australia). High-resolution MR structural images were acquired using a 16.4 Tesla (700 MHz) vertical wide-bore microimaging system interfaced to an AVANCE I spectrometer running imaging software Paravision 6.0.1 (Bruker Biospin, Karlsruhe, Germany) in the Centre for Advanced Imaging at the University of Queensland. Imaging was performed at room temperature (22°C) using a circulating water-cooling system. Three dimensional high resolution structural images were acquired using fast low angle shot (FLASH) with the following parameters based on (Chung et al., 2020): echo time (TE)/repetition time (TR) = 12/40 ms, average = 4, flip angle (FA) = 30°, field of view (FOV) = 7.2 mm × 6.4 mm × 8 mm to 9 mm× 8 mm × 18 mm for different individuals, 30 μm isotropic resolution. Total acquisition time for one sample was 8 h (smallest sample) to 19.3 h (largest sample). All images were analysed using

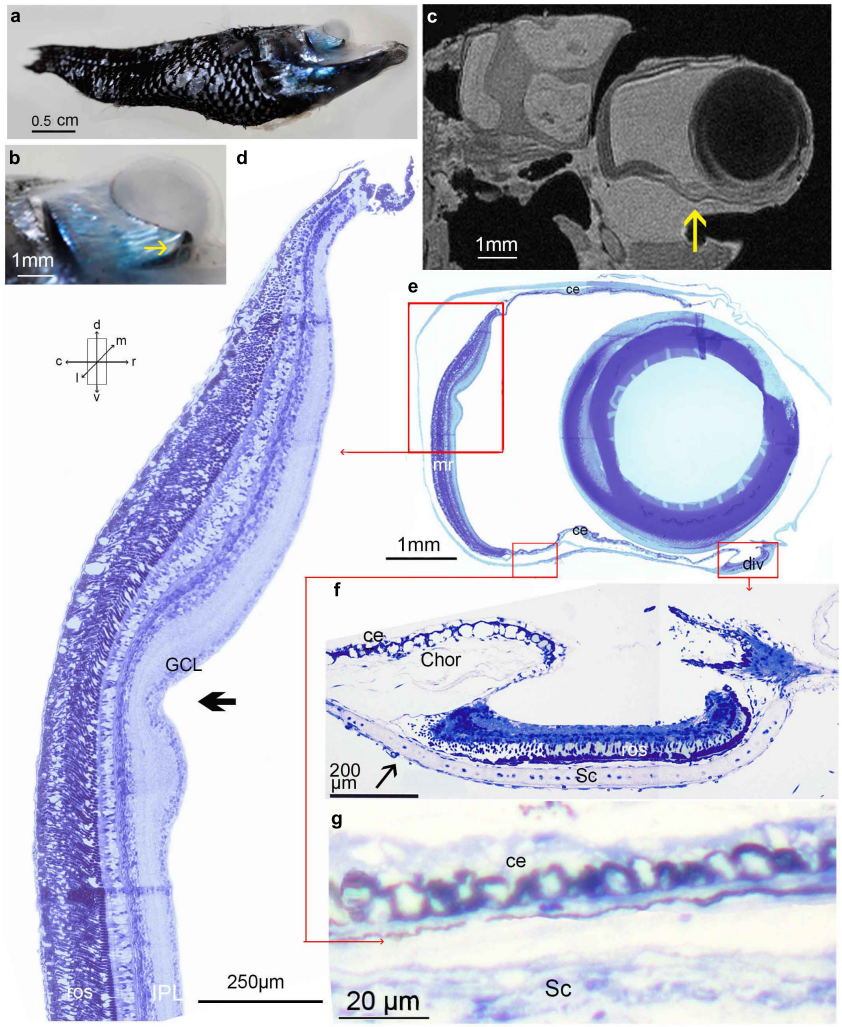

FIGURE 2
Winteria telescopa: **(a)** side view of entire animal (SL 42 mm); **(b)** higher power view of the right eye, arrow indicates diverticulum; **(c)** MRI scan in the sagittal plane, arrow indicates diverticulum; **(d)** radial semithin section of the main retina, arrow indicates a marked depression in the retina, located approximately 1.1 mm from the dorsal rim; **(e)** semithin, approximately sagittal, section of the tube eye with lens probably artifactually displaced caudally; **(f)** radial semithin approximately sagittal section of the diverticulum. Note the thinning of the RPE caudally indicated by an arrow, which represents the transparent 'window'; **(g)** non-photosensitive ciliary epithelium of the ventral wall of the tube eye; a regular accessory retina is present on the medial wall which is not in this plane of sectioning. The orientation arrows shown are applicable to all panels but see Materials and Methods for comments on deviations from the horizontal plane in histological sections.

MRtrix3 (version 3.0.2, open-source software[1]) (Tournier et al., 2019).

Phylogeny

A phylogeny comprising 10 species of Opisthoproctidae and 7 outgroup species was reconstructed using available data on Genbank. In total we targeted 15 mitochondrial genes, and four nuclear protein coding genes. We obtained mitochondrial sequences from available mitochondrial genes using the R package AnnotationBustR v1.30 (Borstein and O'Meara, 2018), augmented with additional sequences obtained from Genbank. Alignments were then made for individual genes with Clustal Omega v1.2.4 using an EMBL-EBI server[2]. Sequence names were standardised, and the alignments were concatenated using SequenceMatrix v1.8 (Vaidya et al., 2011). In total this resulted in an alignment of 17,700 base pairs, including 14,087 base pairs of mitochondrial loci and 3,613 base pairs of nuclear loci. The analysed matrix was 73% complete. We partitioned

1 http://www.mrtrix.org/

2 https://www.ebi.ac.uk/Tools/msa/clustalo/

the matrix into each codon position of protein coding loci, and for the entirety of non-protein coding loci. We then determined the most appropriate models for each partition using PartitionFinder2 (Lanfear et al., 2017). Next, we used RaxML-NG v. 0.9.0 (Kozlov et al., 2019) with a partitioned model, to resolve the most likely phylogeny, with branch support estimated from 100 bootstrap replicates.

Results

This section contains novel data generated in this study. A summary of previous findings relating to tube eyes in general (SM1) and the *D. longipes* and *R. natalensis* used here have been placed in the **Supplementary Material** (**Supplementary 2, 3**).

Opisthoproctus soleatus

Superficially, the eyes of *O. soleatus* (**Figures 1b–d**) are similar to those of other mesopelagic fish with tubular eyes (**Supplementary Material 1**). The base of each eye is covered by a well-developed main retina (**Figures 1c–e**), which in our specimen is about 280 μm thick, around 70% of this consisting of four tiers of rod inner and outer (length 25 μm) segments. Interestingly, the inner and outer tiers have thicker diameter outer segments (5 μm) than those in the intermediate layers (3 μm). There also appears to be more than a single layer/type of horizontal cell in the inner main retina. About 1/3rd of the way up the medial wall (**Figure 1c**), the main retina transforms into the less well-developed accessory retina with reduced photoreceptors and inner retinal layers. In the mediocaudal region adjacent to the base of the iris, the accessory retina shows a marked thickening to twice its original width for a length of about 300 μm. Laterally, the structure of the main retina also changes and resembles the peripheral proliferation zone of other teleosts with spherical eyes: the rod outer segments disappear, as well as the plexiform layers, and numerous small, poorly differentiated cells form a dense cluster (**Figure 1h**). The lateral wall of the tube eye resembles a ciliary epithelium with a persisting pigment epithelium and one or two layers of perikarya which are not differentiated into photoreceptors and/or neurons (**Figure 1h**). Due to the orientation of the sections, the transition from accessory retina to ciliary epithelium in the rostral and caudal walls of the tube eye, both here and in the other species discussed below, is cut tangentially and could therefore not be precisely determined.

The most notable departure of the *O. soleatus* eye from a conventional tube eye is that near the rostrolateral dorsal rim of the tube eye, the ciliary epithelium is replaced by a small area of retina, extending approximately 350 μm from its dorsal to ventral edges, located about 0.5 mm ventral of the sclerocorneal junction (**Figures 1c,d,f,g**). The retina within this diverticulum is more developed than the accessory retina covering most of the medial wall but less extensive than the ventral main retina. There is also marked asymmetry in the organisation of the diverticular retina: Ventrally, it has only one or two layers of short rods, whereas the density and length of up to three layers of rod outer segments increases dorsally (**Figure 1f**).

The diverticulum is continuous with the main eye *via* a small ventral opening (**Figure 1f**). Both the lateral surface of the diverticulum external to the retina and the medial wall separating it from the main tube eye, contain irregularly arranged reflective crystals originating from both a retinal tapetum and the choroid (**Figure 1g**). Ventrally within the diverticulum, the choroid and pigment epithelium lack melanosomes and reflective crystals, creating a "window" through which ventrolateral illumination can enter the diverticulum (**Figure 1f**).

As the diverticulum is restricted to the choroid, the pigment epithelium and the retina, and does not include a scleral outfolding, it is not visible externally and the eye appears as a smooth cylinder. Only microscopy reveals its presence.

Winteria telescopa

The structure of the eyes of *W. telescopa* is in most respects similar to that of *O. soleatus*. However, as the eyes of *W. telescopa* are rostrally directed, at least when caught (**Figures 2a–c**), the planes of orientation of their eyes differ from those of the other species discussed here, the eyes of which mainly face dorsally. The cornea and lens in *W. telescopa* are therefore not usually dorsal as in *O. soleatus*, but rostral. Similarly, the base of the tubular eye, which is usually ventral in other species, is caudal in *W. telescopa*, and the "vertical" rostral and caudal walls of the tubular eyes of other species are horizontal, forming the ventral and dorsal surfaces of the eye, in *W. telescopa* (**Figure 2e**).

The main retina of *W. telescopa* in our specimen is 250–280 μm thick and has 2–4 layers of rod outer segments 25–30 μm in length. There is a dorsoventral gradient in the thickness of the main retina (**Figure 2d**) where the thinner part, consisting of 2–3 layers of rods, is dorsal and the thickest region, with 3–4 rod layers, ventral. About 1.1 mm central to the dorsal edge, the main retina shows a depression associated with an increased ganglion cell density and flanked by slight ridges (**Figure 2d**).

When sectioned perpendicular to the diverticulum, the ventral and dorsal walls of the tubular eye are lined by a two-layered ciliary epithelium (**Figure 2g**) lacking photoreceptors. As in *O. soleatus*, the transition between the main retina and the ciliary epithelium is marked by a proliferation zone. Serial sections show that, as in most tubular eyes, the medial wall of the *W. telescopa* eye is lined by an accessory retina with a single layer of short rods and thin inner layers, whereas the lateral wall is covered with the ciliary epithelium. Also, as in *O. soleatus,* there

is a thickening of the accessory retina close to the sclerocorneal junction rostromedially.

The diverticulum of *W. telescopa* is located ventrolaterally near the corneoscleral junction (**Figure 2b**). Although structurally very similar to the diverticulum of *O. soleatus*, due to the different orientations of the eyes in the two species, the part of the visual field they sample differs. While *W. telescopa* has an unpigmented window similar to *O. soleatus*, which is clearly visible externally, it is located caudal to the diverticulum in *W. telescopa* (**Figure 2f**) and therefore samples the caudolateral visual field, while the ventral positioning of the window in *O. soleatus* enables sampling of the ventrolateral visual field. The microscopic organisation of the diverticular retina in *W. telescopa* is also similar to *O. soleatus*, showing a rostrocaudal asymmetry and communicating with the main tubular part of the eye *via* a small opening (**Figure 2f**). However, unlike in our specimen of *O. soleatus*, the diverticulum of *W. telescopa* includes a scleral outfolding and is therefore visible externally without microscopy or sectioning. The outer diameter of the diverticulum in our specimen is about 900μm, equivalent to 15% of the ocular length.

Dolichopteryx longipes

Histological examination and mathematical modelling of a single eye from a large (SL 102 mm) *D. longipes* has previously shown it to consist of an approximately dorsally directed tubular portion with a well-developed, complex, lateral diverticulum (Wagner et al., 2009; **Supplementary Material 2**). Here we present further histological observations on the eye of this specimen, describing the connection between the diverticulum and the tubular portion of the eye and quantifying the retinal ganglion axons leaving both the diverticulum and the tube eye. We also present MRI scans of two smaller individuals (SL 93 and 52 mm) to confirm the earlier histological findings and examine any developmental change in ocular structure.

While external observation (**Figures 3a,b**) and MRI scans (**Figures 3c,e,g**) of the 93 mm specimen confirm the presence of the dorsolateral protruding diverticulum seen externally (**Supplementary Figure 2a**) and in histological section (**Supplementary Figure 2c**) in the 102 mm animal, MRI scans of the smallest, 52 mm, animal (**Figures 3d,f,h**) show a less pronounced diverticulum that does not extend significantly beyond the lateral wall of the eye and is largely contained within its tubular outline.

As shown previously, light enters the diverticulum, at least in larger animals, through a ventrolaterally directed cornea and is redirected by a mirror on its medial surface to form a well-focussed image on the laterally positioned retina (Wagner et al., 2009; **Supplementary Material 2**). All the major features of the *D. longipes* eye previously seen only histologically (**Supplementary Figure 2c**), such as the ventrolateral diverticular cornea and the lateral positioning of the diverticular retina are also clearly visible in MRI scans, especially of the 93 mm animal (**Figure 3g**).

The retina of the main tubular eye and that of the diverticulum are connected, although when sectioned in the centre of the diverticulum they appear separated by a septum (**Supplementary Figure 2c**). However, from reconstructed serial sections (**Figure 4**) and a series of MRI scans (not shown), it is evident that rostrally the diverticular retina is continuous with the accessory retina of the main eye (**Figure 4**, 3rd section). It is through this connection that the retinal ganglion cell axons leave the diverticulum and form a fascicle that runs over the surface of the retina in the tubular eye, ultimately joining the ganglion cell axons of the tubular portion of the eye and forming the optic nerve which leaves the tube eye mediocaudally.

To assess the relative contribution of the diverticulum to the total visual output of the eye, we quantified the proportion of axons in the optic nerve that originated from the diverticulum. Of the 14,182 axons in the optic nerve 25% came from the diverticulum (**Table 2**), although the diverticular retina only had a surface area 15% of that of the main retina within the tubular portion of the eye. Not surprisingly therefore, the average density of ganglion cells in the diverticulum was approximately more than twice the average density of ganglion cell in main retina (**Table 2**).

Rhynchohyalus natalensis

As described elsewhere (Partridge et al., 2014; **Supplementary Material 3**), the eye of adult *R. natalensis*, like that of *D. longipes*, is bipartite, consisting of a dorsally directed tubular portion and an extensive, mainly laterally directed, diverticulum (**Supplementary Figures 3a–e**). The diverticulum has a reflective medial wall (**Supplementary Figure 3l**) that redirects light entering the diverticulum through a transparent, ventrolaterally directed cornea (**Supplementary Figures 3b–e,i**) onto a well-developed, laterally positioned, retina (**Supplementary Figures 3c–f**). Here we describe how the diverticulum and the tubular portion of the eye are connected and assess the relative contribution of the diverticulum to the eye's total output by comparing the number of axons within the fascicle exiting the diverticulum to the total number of axons in the optic nerve.

The axons of diverticular retinal ganglion cells converge towards the ventrocaudal region of the diverticulum, where they form a ribbon-like fascicle that exits the diverticulum through an aperture in the septum separating it from the tubular portion of the eye (not shown). This bundle of diverticular ganglion cell axons becomes associated with the accessory retina of the tube eye and joins the chorionic fissure, terminating at the optic nerve head, which is located mediocaudally in the medial wall of the tube eye, about 2 mm dorsal to the bottom of the tube. Here

10.3389/fevo.2022.1044565

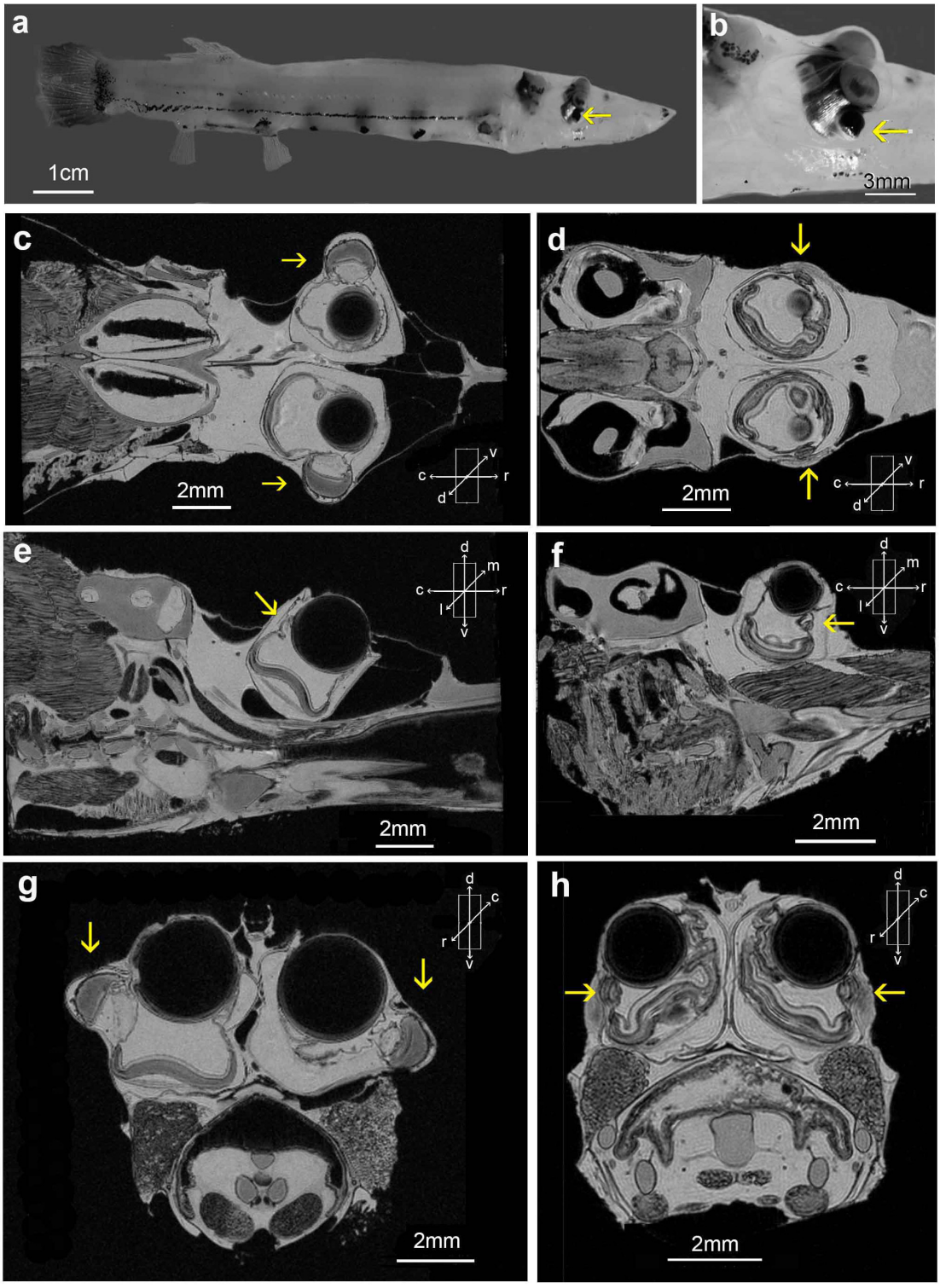

FIGURE 3
Dolichopteryx longipes **(a,b)** side views of an animal with SL 93 mm; **(c,e,g)** MRI scans from this specimen; **(d,f,h)** equivalent scans from a smaller animal (SL 52 mm). MRI scans were taken at the central level, where lens diameter is maximal, of the left tube eye in the sagittal **(e,f)**, and transverse **(g,h)** planes. MRI scans in the horizontal plane **(c,d)** were taken at the level best illustrating the diverticula. Yellow arrows indicate diverticula.

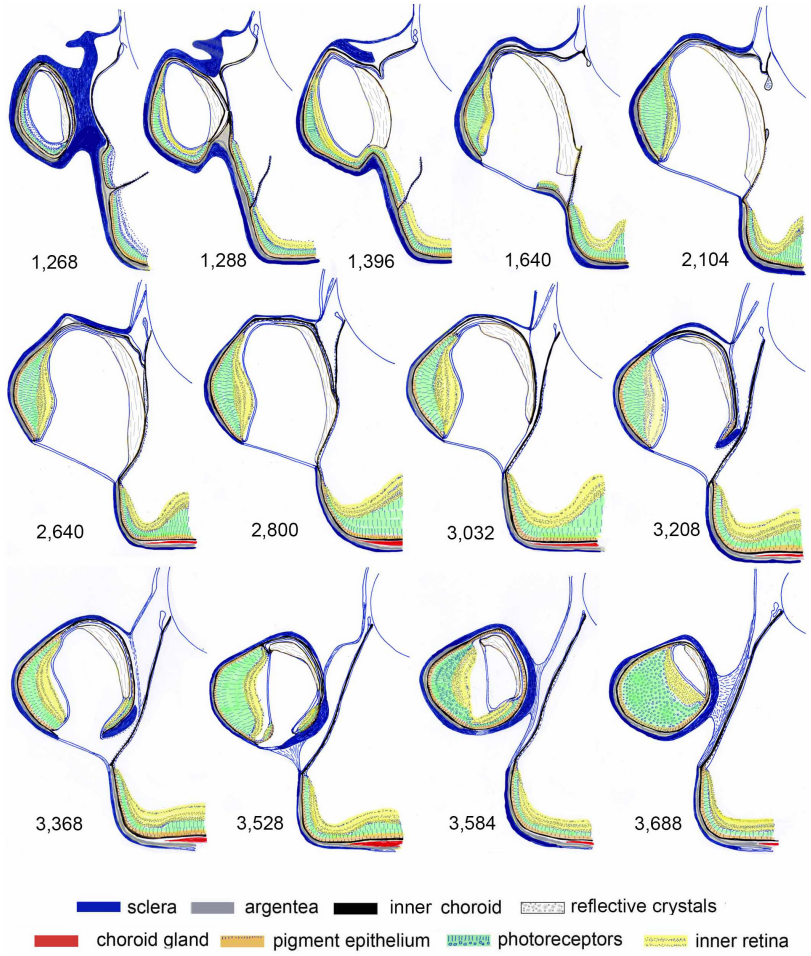

FIGURE 4
Schematic representation of serial sections through the diverticulum of *Dolichopteryx longipes*. 2 μm transverse sections were cut starting rostrally at a spacing of 4 μm through the diverticulum of a large animal (SL 102 mm). The numbers indicate the distance in μm from the rostral edge of the eye.

the ganglion cell axons from the main eye and the diverticulum combine and exit the eye in a dorsocaudal direction. About 10mm after exiting the tube eye, the optic nerves from the two eyes cross to the contralateral side at the optic chiasm without apparent exchange of fibres.

Of the 33,125 axons in the optic nerve, 20% came from the diverticulum (Table 2). The diverticular retinal area was 42% that of the main retina in the tube eye, and the average density of ganglion cells in the diverticulum was only 61% of that in the main retina (Table 2).

Bathylychnops exilis

The eye of *B. exilis* examined here consisted of a roughly spherical main globe, with a dorsally positioned cornea and lens collecting light from the dorsolateral field of view, and an extensive rostrolateral diverticulum containing a sclerally derived lens gathering ventrolateral illumination (Figures 5a–d). Both the main globe and the diverticulum are lined with regionally differentially developed retina.

The ventral retina of the main eye, which is structurally similar to the main retina of more tubular eyes, has rods arranged in four layers with no clear region of increased cell density (Figure 5f). Medially the retina of the main eye thins forming an 'accessory retina' containing three layers of more widely spaced and shorter rods (Figure 5g). The diverticular retina (Figure 5e) contains rods arranged in up to four layers and is continuous ventrally and dorsally with the accessory retina of the main eye. The diverticulum and main eye are connected by a large central opening in the cartilage reinforced septum otherwise separating them (Figure 5c). The scleral lens of the diverticulum is ellipsoidal (ca. 1.4 mm × 1.8 mm) and is composed of dense connective tissue organised in mostly concentric lamellae. On the inner face, the scleral lens is covered

TABLE 2 Quantitative analysis of the retinae within the diverticulum and main eye of *Dolichopteryx longipes* (SL 102 mm) and *Rhynchohyalus natalensis* (SL 183 mm).

	D. longipes	*R. natalensis*
Area of main retina (mm^2)	12.60	346.30
Area of diverticular retina (mm^2)	1.95	143.75
Axons in optic nerve	14,182	33,125
Axons in diverticular fascicle	3,487	6,750
Mean GC density main retina (mm^{-2})*	849	76.2
Mean GC density diverticular retina (mm^{-2})	1788	47.0

*This calculation, obtained from subtracting the number of axons in the diverticular fascicle from the total number of axons in the optic nerve, divided by the area of the main retina is an approximation as it assumes that all axons in the optic nerve not emanating from the diverticulum will have their origin in the main retina of the tubular portion of the eye. As the optic nerve also contains efferent fibres, as well as fibres coming from the accessory retina of the tubular eye, the calculated ganglion cell density for the main retina will be an overestimate. However, as the ganglion cell density in the accessory retina is very low compared to in the main retina (Collin et al., 1997) and the number of efferent fibres is also limited (Wagner et al., 1998), the error will be small.

by a thin, unpigmented, double layered ciliary epithelium that is derived from the diverticular retinal pigment epithelium and the neural retina (**Figures 6a–d**).

In the laterocaudal wall of the diverticulum, the sclera shows a marked thickening that is continuous with the sclera of the main eye and forms an ellipsoidal swelling approximately 1mm thick, 2 mm wide and 2.5 mm high (**Figures 5a,b**, **6e,f**). This structure, which previous authors (Pearcy et al., 1965; Munk, 1966) have called a 'corneal projection' despite the fact it does not seem to be associated with the cornea, is covered on its inner surface by the choroid and ciliary epithelium of the main eye (**Figures 6f–i**). Since the former is pigmented (**Figure 6h**) and the ciliary epithelium consists of a prominent pigment epithelium as well as a transparent layer of cells without any differentiated photoreceptors (**Figure 6i**), the 'corneal projection' is separated from the main eye by two dense aggregations of melanosomes.

Macropinna microstoma

The eyes of *M. microstoma* used in this study were fixed in paraformaldehyde and ethanol, which makes detailed histology, especially in the larger animal, difficult. However, since such material is scarce, we give a brief, preliminary, outline of the major characteristics of the *M. microstoma* eye.

In the following description the tubular portion of the eye is assumed to be dorsally directed, although the eyes are capable of significant dorsorostral rotation (Robison and Reisenbichler, 2008). We examined the left eyes of two individuals (SL 32 and 55 mm). Although the main retina covering the base of the tubular eyes was similar in both animals, containing several banks of rods with no obvious regional specialisations (**Figures 7c**, **8h**), their rostrolateral diverticula were developed to different degrees.

The diverticulum in the smaller eye (**Figures 7a,b,d**) in many ways resembles those of *O. soleatus* (**Figure 1f**) and *W. telescopa* (**Figure 2f**), consisting of an area of lateral retina containing a single layer of rods just ventral to the corneoscleral junction. However, in *M. microstoma* it is somewhat larger than in these other species, measuring around 1000μm in the dorsoventral direction and occupying about half of the lateral wall. In our sections of this animal, unlike in *O. soleatus* and *W. telescopa*, there was no evidence of a ventrolateral unpigmented 'window' although it is probable it does exist and was simply not seen as it was located out of the plane of the sections.

The diverticulum of the larger specimen is more developed than in the smaller animal and clearly visible externally in a freely swimming adult (**Figure 8a**) and is also apparent in MRI scans (**Figure 8b**) and histological section (**Figures 8c,e,f**). The retina of the diverticulum, which contains two layers of rod outer segments and very few ganglion cells (**Figures 8e–g**), is located dorsally in the dome-shaped apex of the diverticulum. The medial wall of the diverticulum (**Figure 8i**) is composed of a two layered ciliary epithelium derived from the neural retina and the retinal pigment epithelium, and internally the choroid. Cells within this septum, as in *R. natalensis* (**Supplementary Material 3**) contain empty spaces ('ghosts') where we think reflective crystals were most likely located prior to fixation (**Figures 8i,j**). These reflective cells, also as in *R. natalensis*, are located within the choroid. A diverticular collagenous cornea, bounded externally by a simple, flat epithelium, and internally by a thin layer of fibroblasts with no clear basement membrane, is positioned ventrally. As there is a marked increase in thickness at its lateral border with evidence of blood vessels, it is likely that the diverticular cornea of the larger animal only permits ventral illumination into the diverticulum.

Phylogenetic relationships

Our phylogenetic reconstruction based on 15 mitochondrial loci and four nuclear protein coding genes (**Figure 9**), recovered a monophyletic Argentiniformes, comprising all Argentinidae, Bathylagidae, Microstomatidae, and Opisthoproctidae. The immediate sister clade to the Opisthoproctidae was resolved as the Argentinidae (*Argentina* and *Glossanodon*). The nine members of the Opisthoproctidae sampled comprised a monophyletic clade, and the within this clade the short-bodied genera were resolved as monophyletic, with the long-bodied genera occupying basal positions. The short-bodied species group was resolved as a monophyletic group of the soled genera (*Monacoa* and *Opisthoproctus*), but the relationships of the non-soled genera (*Winteria*, *Macropinna,* and *Rhynchohyalus*) to one another, and to the clades of soled species, were unresolved.

10.3389/fevo.2022.1044565

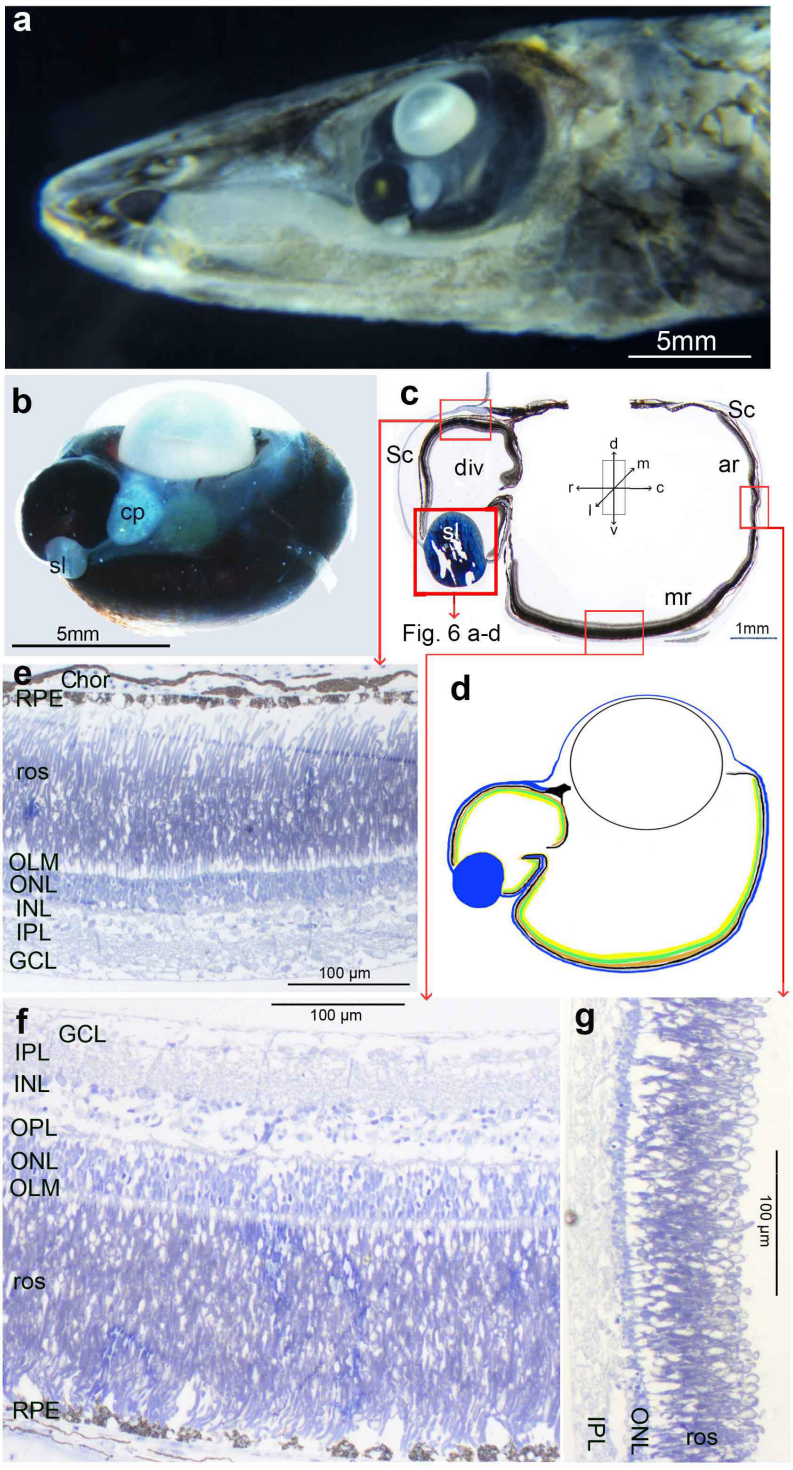

FIGURE 5

Bathylychnops exilis: **(a)** Head of an adult specimen (SL 200 mm); **(b)** Isolated eye showing the rostrolateral diverticulum with a ventral scleral lens, and a caudal 'corneal projection'; **(c)** Thick section of the left eye showing the main globe and the diverticulum. The cornea of the main eye has been removed and during preparation the retina lining the diverticulum has become detached from the sclera laterally; **(d)** Schematic of an approximately transverse section of the eye colour coded as in Figure 1; **(e)** Radial semithin section of the retina in the dorsal diverticulum; **(f)** radial semithin section of the main retina; **(g)** radial semithin section of the accessory retina. The orientation arrows shown in panel **(c)** are applicable to all panels but see Materials and Methods for comments on deviations from the transverse plane in histological sections.

10.3389/fevo.2022.1044565

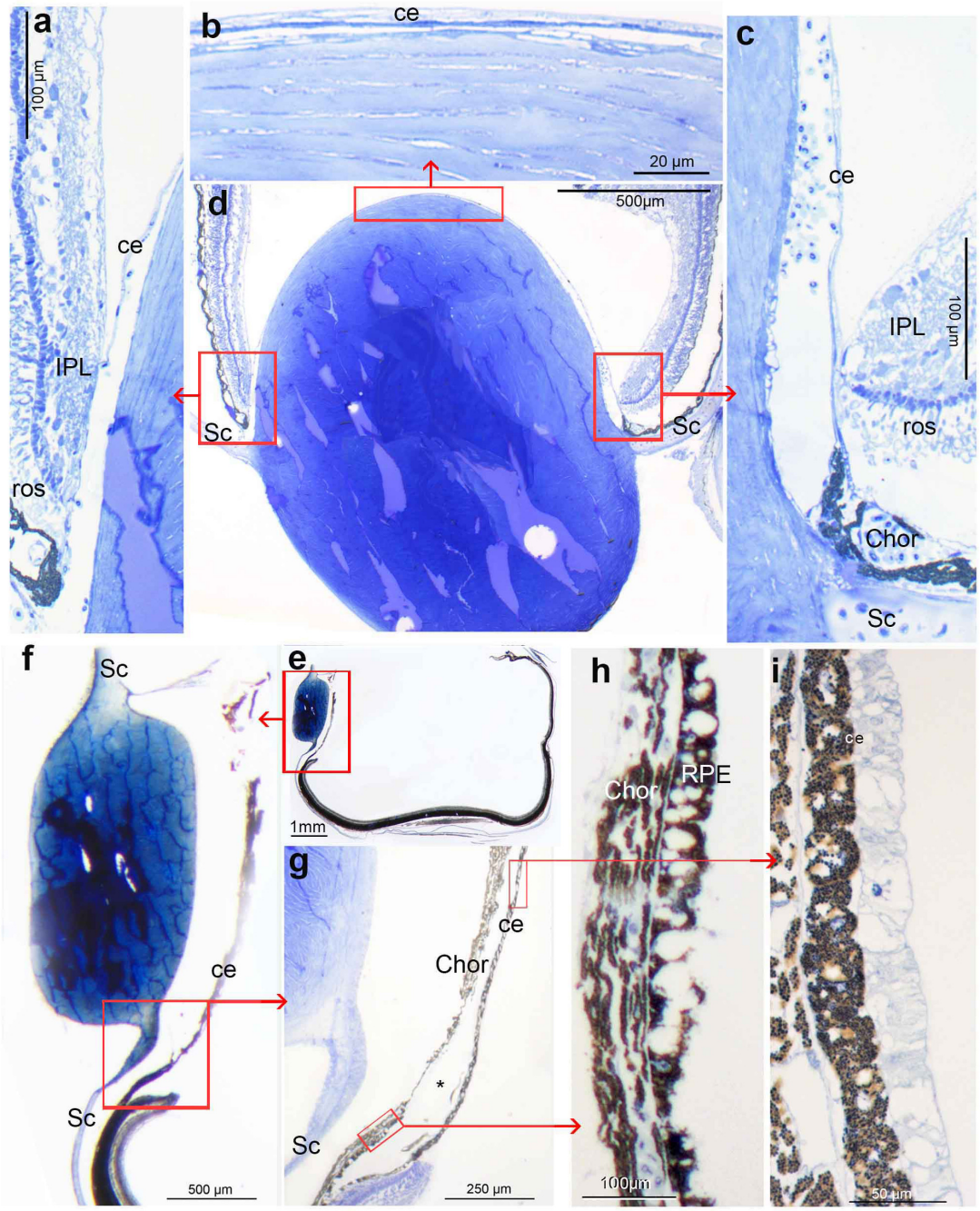

FIGURE 6
Bathylychnops exilis: **(a–d)** semithin sections of the areas around the scleral lens within the ventral diverticulum in the same orientation as indicated in **Figure 5**; **(a)** rostrolateral retina and scleral lens; **(b)** high power light micrograph of the dorsal region of the diverticular scleral lens; **(c)** semithin section of the retina adjacent to the lens mediocaudally; **(d)** lower power micrograph of the whole lens, the internal surface of which is covered by a thin ciliary epithelial layer derived from the retinal pigment epithelium and neural elements of the adjacent retina. The continuity of the lens and the sclera is evident in panels **(c,d)**; Sections **(e–i)** show areas of the eye adjacent to the corneal projection and are taken from a more caudal plane than those shown above. **(e)** Thick section of the eye; **(f)** semithin section of the corneal projection; **(g)** caudal aspect of the corneal projection with transition to the sclera and choroidal tissue as well as ciliary epithelium covering it on the inner face. *Indicates an artefactual separation of the layers; **(h,i)** high power micrographs of the choroid and ciliary epithelium internal of the corneal projection, both of which show a high degree of pigmentation suggesting light cannot enter the eye by this route. The ciliary epithelium consists of a continuation of the retinal pigment epithelium and a transparent layer of non-photoreceptive cells.

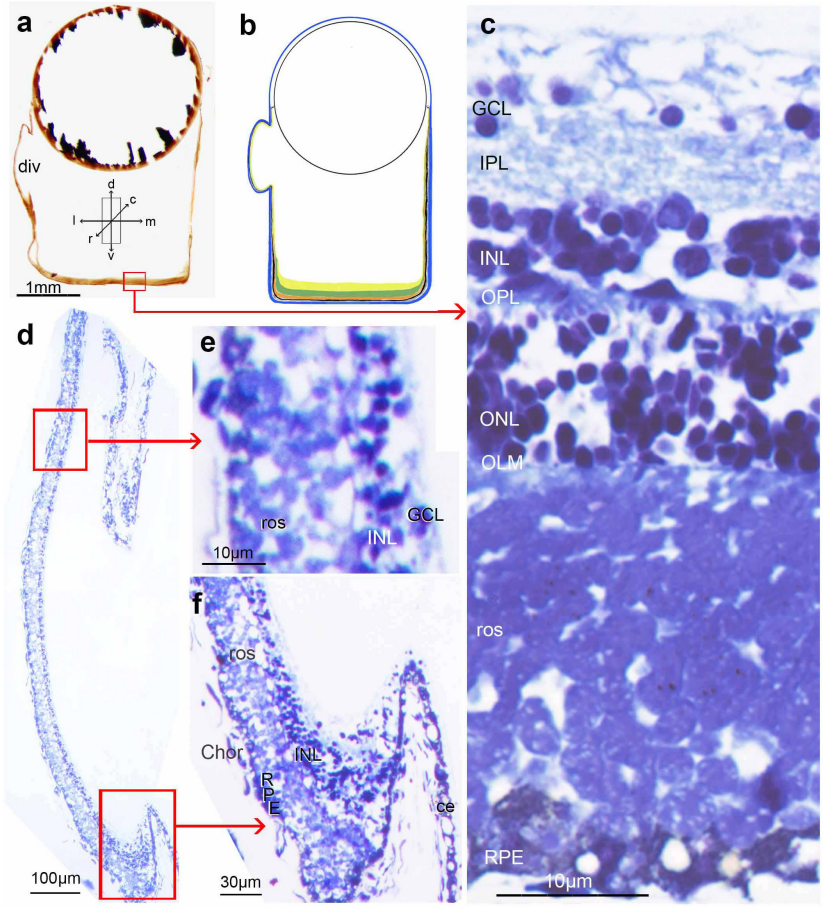

FIGURE 7
Small *Macropinna microstoma*: **(a)** approximately transverse thick section of tube eye (all but the peripheral lens was lost during sectioning); **(b)** schematic drawing of tube eye with diverticulum, colour coded as **Figure 1**; **(c)** semithin radial section of the main retina; **(d)** radial semithin section of the diverticulum; **(e)** radial section of the central retina of the diverticulum; **(f)** semithin section of the ventral area of the diverticulum with transition to the tube eye wall, where the diverticular retina changes to a ciliary epithelium. The orientation arrows in panel **(a)** are applicable to all panels but see Materials and Methods for comments on deviations from the transverse plane in histological sections. All images in this figure came from an animal of SL 32 mm.

Discussion

Diversity of ocular structure among the Opisthoproctidae

Eyes with simple diverticula (*Opisthoproctus soleatus*, *Winteria telescopa,* and *Monacoa grimaldi*)

We, and others (Brauer, 1908; Munk, 1966; Collin et al., 1997) have described essentially similar tubular eyes with relatively simple, retina-containing, diverticula close to the iris root in the lateral walls of *O. soleatus* and *W. telescopa*. Very similar eyes have also been described in *O. grimaldi* (Munk, 1966; Collin et al., 1997), which is now placed in the genus *Monacoa* along with two newly described species (Poulsen et al., 2016). In most respects, our observations broadly agree with previous descriptions. Thus, the location, size and morphology of the small lateral diverticula and their connection to the rest of the eye are similar in this and previous studies, as is the general arrangement of the main and accessory retinae in the rest of eye. However, there are some differences between our work and that of others.

For example, while we observed four tiers of rod outer segments in the main retina of *O. soleatus*, Collin et al. (1997) saw only one. This might suggest that, as described in other species with tubular eyes (**Supplementary Material 1**), there are regional differences in the structure of the main retina. Alternatively, the number of tiers of photoreceptors is known to increase with age/size in some species (Locket, 1980; Frőhlich and Wagner, 1998), and the individual examined here (SL 42 mm) was exactly twice as big as that studied by Collin et al. (1997).

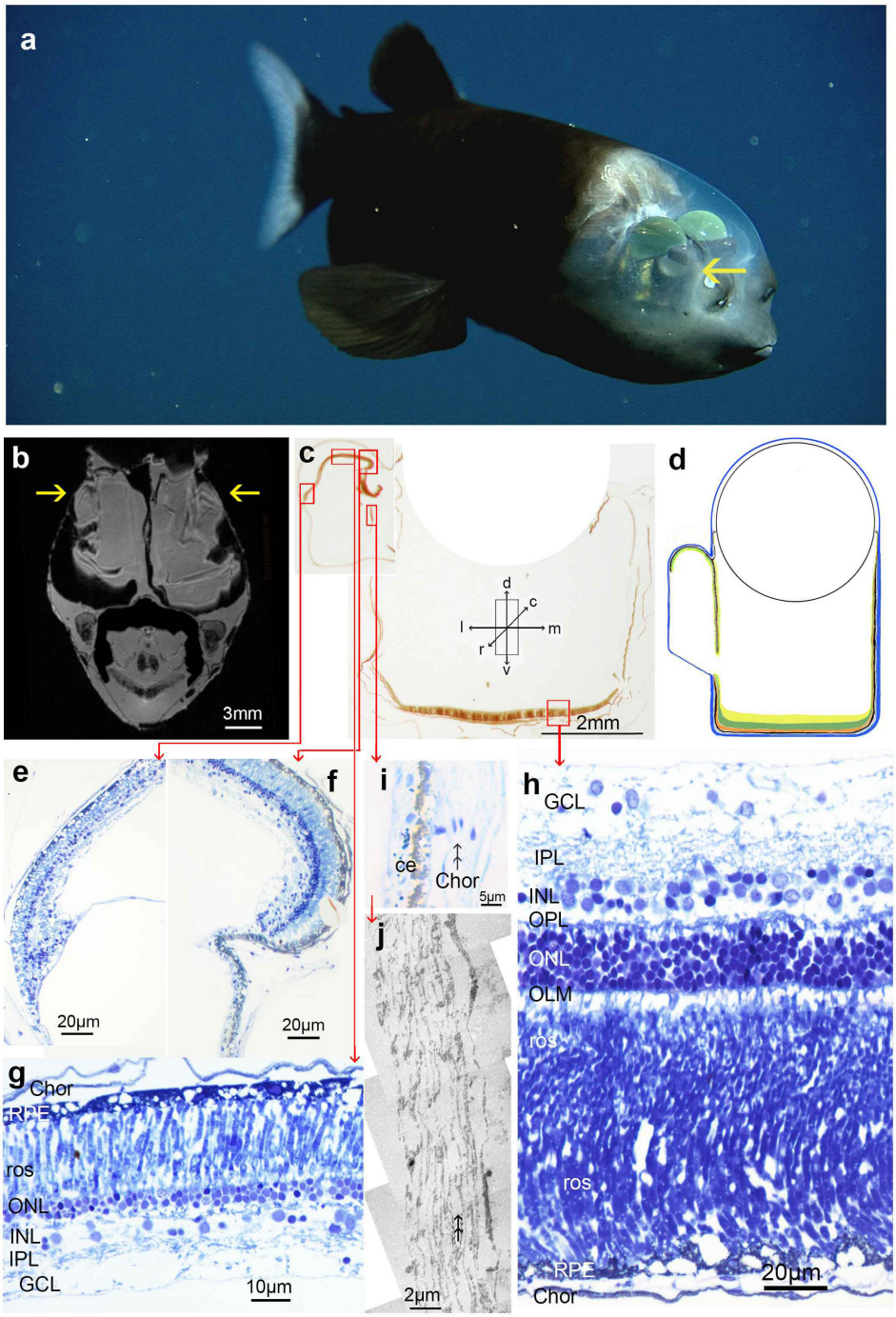

FIGURE 8
Larger *Macropinna microstoma*: **(a)** image of an animal (SL 110 mm) obtained using an ROV [reproduced from Robison and Reisenbichler (2008) with permission from the American Society of Ichthyologists and Herpetologists]. Arrow indicates the rostrolateral diverticulum; **(b)** MRI scan in a transverse plane, arrows indicate diverticula; note marked artificial folding of the retina following chemical fixation with aldehydes; **(c)** approximately transverse thick section of tube eye with lens removed. Due to the poor histology of this animal, the eye is illustrated with a composite of two sections, one of the diverticulum and one of the tubular portion of the eye; **(d)** schematic drawing of tube eye with diverticulum, colour coded as in **Figure 1**; **(e,f)** radial semithin sections of the lateral **(e)** and medial **(f)** areas of the diverticulum; **(g)** radial section of the dorsal retina of the diverticulum; **(h)** semithin radial section of the main retina of the tube eye; **(i)** radial semithin section of the septum between the diverticulum and the tube eye; **(j)** radial low power electron micrograph of the septum between the diverticulum and the tube eye; the double arrows in panels **(i,j)** point at "ghost" spaces where reflective crystals (likely guanine) lost during preparation may have been located. The orientation arrows in panel **(c)** are also applicable to panels **(d–h)** but see Materials and Methods for comments on deviations from the transverse plane in histological sections. All images in this figure came from an animal of SL 55 mm, except for the animal shown in panel **(a)**.

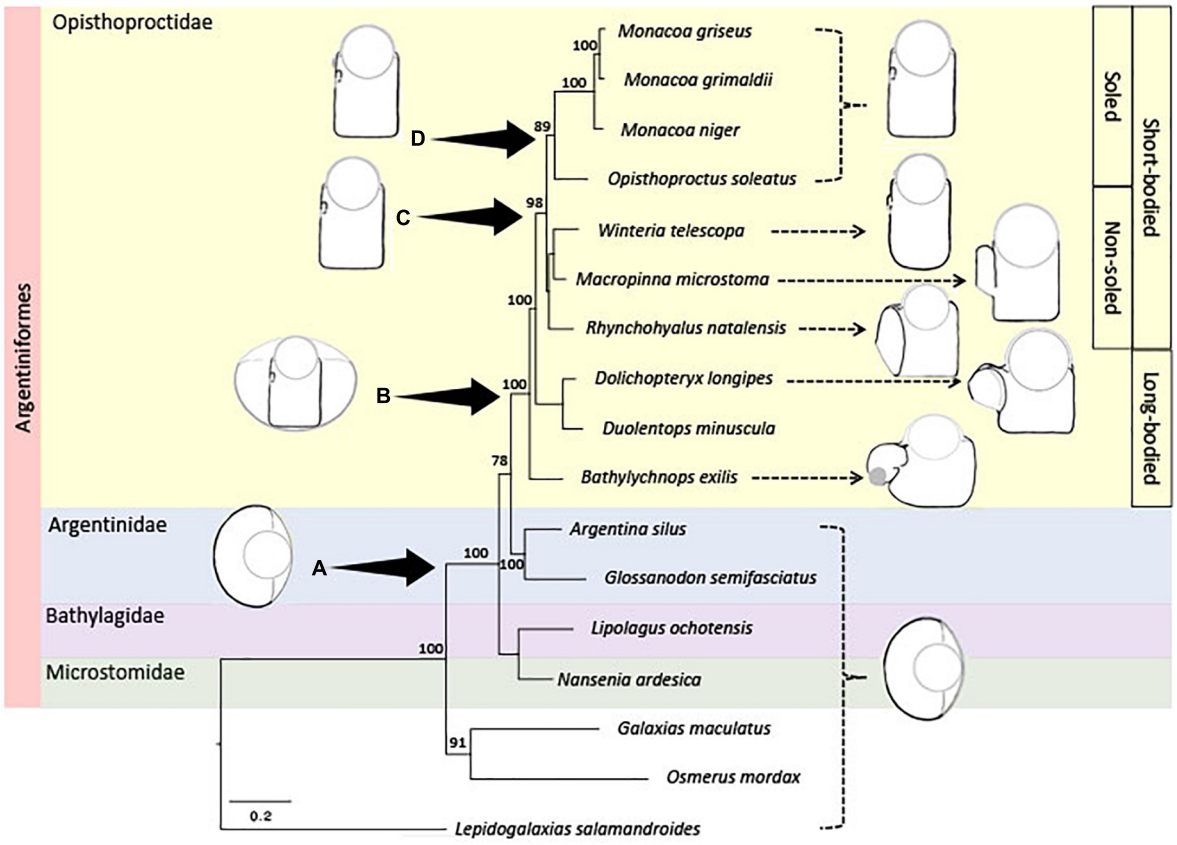

FIGURE 9
Maximum-likelihood phylogeny of Opisthoproctidae: This is based on 15 mtDNA and 4 nuclear loci. Numbers on branches indicate percentage bootstrap support, only values >70 are shown. Nodes **A–D** represent the common ancestors to all: Argentinifomes **(A)**, Opisthoproctidae **(B)**, short-bodied Opisthoproctidae **(C)**, and sole-bearing Opisthoproctidae **(D)**, respectively. *Duolentops miniscula* was previously classified as *Dolichopteryx miniscula* (Prokofiev, 2020) and *Monacoa grimaldi* was formerly *Opisthoproctus grimaldi* (Poulsen et al., 2016). Outlines of the adult eye types of extant species are indicated on the right and the presumed morphology of ancestral species shown on the left. The tube eye shown at node **B** is superimposed on a more spherical eye to illustrate how a tubular eye is equivalent to a peripherally reduced spherical one (Locket, 1977). The scale bar represents a measure of genetic distance.

In contrast to Collin et al. (1997) and Brauer (1908), we observed two morphological classes of rod in the main retina of *O. soleatus* as well as several layers of horizontal cells. Similarly, Brauer (1908) observed two structurally distinct rods in *W. telescopa* while we did not. The presence of morphologically distinct photoreceptor types and/or multiple layers of horizontal cells is consistent with the possession of more than one spectral type of visual pigment. However, only a single pigment has been isolated from the retina of *O. soleatus* during partial bleaching of extracts (Denton and Warren, 1957; RHD pers. obs.), while the visual pigments of *W. telescopa* remain undescribed.

The depression associated with a high ganglion cell density in the main retina of *W. telescopa* (**Figure 2d**), not seen previously in this species, may represent a fovea with increased resolving power, similar to that described in some other deep-sea fish (Locket, 1977; Wagner et al., 1998). However, we cannot rule out that this feature is caused by differential shrinkage of the sclera compared to the retina, although, as it is also associated with an increased ganglion cell density, this is unlikely.

The generally poorly developed accessory retina, covering the eye medially, is thickened near the root of the iris in both *O. soleatus* and *W. telescopa*. A similar asymmetry in the accessory retina is present in other tubular eyes (e.g., *Vinciguerria poweriae* Locket, 1977; *Evermanella balbo* Wagner et al., 2019; *Argyropelecus affinis* **Supplementary Figure 1**; *R. natalensis* **Supplementary Figures 3d,h**).

Although the main retina of most tube-eyed fish is positioned such that the ocular lens conforms to Matthiessen's ratio and thus receives focussed illumination, the accessory retina, including that in the rudimentary diverticula of *O. soleatus*. *M. grimaldi* and *W. telescopa*, is too close to the lens for the light to be focussed (**Supplementary Material 1**). Furthermore, the amount of light entering the diverticulum from the tubular portion of the eye is minimised by a pigmented septum largely separating the two parts of the eye

(**Figures 1f**, **2f**). Most light coming into the diverticulum will do so directly through the unpigmented ventral (*O. soleatus, M. grimaldi*; **Figure 1f**) or caudal (*W. telescopa*, **Figure 2f**) portion of its lateral wall. Such illumination will impinge on the scleral part of the outer segments adjacent to the window first. As pointed out by Brauer (1908), this is in the opposite direction to all other vertebrates. Any light entering this lateral window and not absorbed directly by the photoreceptors will strike the reflective medial wall that separates the diverticulum from the main tubular part of the eye and be reflected onto the retina lining the diverticulum laterally in the 'normal' direction. In other opisthoproctids, with larger and more complex diverticula, we have suggested that regularly arranged reflective crystals (possibly guanine) form plate-like structures in the medial septum producing a mirror that results in focussed images on the lateral retina of the diverticulum (Wagner et al., 2009; Partridge et al., 2014; **Supplementary Material 2, 3**; see below). However, in *O. soleatus* and *W. telescopa*, the reflective crystals in the medial diverticular wall are not abundant and are irregularly arranged, so any role in image formation is unlikely. The lateral illumination entering the diverticulum and impinging on the retina in *O. soleatus*, *M. grimaldi,* and *W. telescopa* through their unpigmented windows will therefore most likely be involved in simple light detection and these species will not benefit from the perception of increased detail and sensitivity within their diverticula that a focussed image would provide (**Figures 10a,b**).

Eyes with complex reflective diverticula (*Dolichopteryx longipes* and *Rhynchohyalus natalensis*)

We have previously shown that larger *D. longipes* (Wagner et al., 2009; **Supplementary Material 2**) and *R. natalensis* (Partridge et al., 2014; **Supplementary Material 3**) have extensive lateral diverticula. In contrast to the diverticula of *M. grimaldi*, *O. soleatus,* and *W. telescopa*, described above, which are small and most likely serve a simple light-detecting function, the larger diverticula of both *D. longipes* and *R. natalensis* produce focussed illumination even in the absence of a lens. In both species, the retina within the diverticulum is absent medially and most well-developed laterally (**Supplementary Figures 2c,g, 3d**). Thus, illumination entering the ventrolaterally facing diverticular window (**Supplementary Figures 2b,c,g, 3b,c,d,i**) will not be absorbed by the retina directly, instead impinging on the retina-free medial wall. In both species the medial wall contains reflective plates which, mathematical modelling has shown produce a well-focussed image on the lateral diverticular retina (**Figures 10e,f** and **Supplementary Figures 2h, 3m**).

Although superficially similar, the medial diverticular mirrors of *D. longipes* and *R. natalensis* produce images in quite different ways and have different origins. In *D. longipes*, the reflective surface is derived from the retinal tapetum and the angles of the reflective plates change progressively around the mirror, forming a Fresnel-type reflector (Wagner et al., 2009; **Supplementary Figure 2h**). In *R. natalensis*, in contrast, the reflective plates arise from the choroid and are orientated almost parallel to the mirror's surface and image formation is thus dependent on the shape of the mirror (Partridge et al., 2014; **Supplementary Figure 3m**). Although image formation by reflection is not uncommon within invertebrates (Land, 1972, 1980, 2000; Vogt, 1980; Land and Nilsson, 2012), the diverticula of *D. longipes* and *R. natalensis* are the only known examples of reflective optics in vertebrates.

In both *D. longipes* and *R. natalensis* the ganglion cells of the diverticular retina form a discrete fascicle that exits the diverticulum through an aperture in the septum separating it from the tubular portion of the eye (e.g., **Figure 4** 3rd section). This fascicle runs over the surface of the accessory retina before eventually aggregating with the ganglion cell axons from the accessory and main retinae of the tube eye to form the optic nerve. To assess the relative contribution of the diverticulum to the total ocular output, we determined the area of, and ganglion cell density within, both the diverticulum and the main retina of the tube eye and compared the number of axons in the diverticular optic fascicle to the total number of nerve fibres within the optic nerve.

The size of the eye of the *R. natalensis* examined was approximately five times the height and width of that of the largest *D. longipes* (**Table 1**). Therefore, not surprisingly, the surface areas of both the diverticular and main retina were far larger in *R. natalensis* (**Table 2**). Furthermore, as the diverticulum of *D. longipes* is comparatively small and restricted to the dorsal half of the lateral wall of the tube eye (**Figure 3b** and **Supplementary Figure 2c**), the diverticular retina area is only 15% the size of the main retina. In *R. natalensis*, however, the diverticulum is far larger, extending over the entire lateral flank of the tube eye (**Supplementary Figures 3c–e**) and consequently its retina has a surface area 42% that of the main retina (**Table 2**).

Although the area of the diverticular retina in *D. longipes* is small (15%) compared to the area of the main retina in the tube eye, it accounts for 25% of the axons in the optic nerve (**Table 2**). While in *R. natalensis*, even though the diverticular retina is relatively much larger (42%) compared to the main retina, it contributes only 20% to the eye's output (**Table 2**). Furthermore, the diverticular retina of *D. longipes* has 211% the average density of ganglion cells compared to the main retina of the tube eye. In *R. natalensis* the corresponding value is reduced to 62%. Both the relatively high contribution of the diverticulum to the eye's output despite its small size and the relatively higher average ganglion cells density within it, implies that the diverticulum in *D. longipes* is functionally more significant than that of *R. natalensis*.

As ganglion cells are the output neurons of the retina, their density is a key determinant of spatial resolution; a higher density leading to increased resolving power. Since the density

10.3389/fevo.2022.1044565

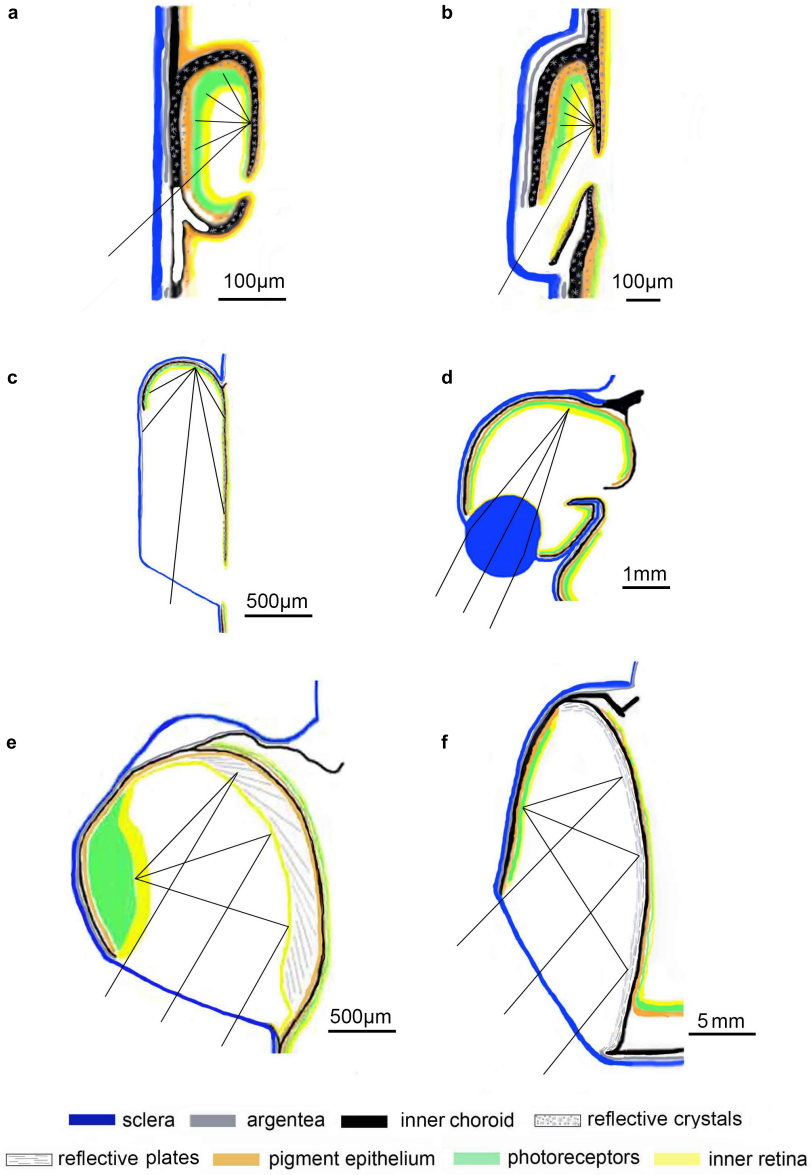

FIGURE 10
Schematic representation of Opisthoproctid diverticula: In all diagrams the main, usually tubular, portion of the eye would be to the right of the diverticulum. The possible path of light rays entering the diverticula are shown; **(a)** *Opisthoproctus soleatus*. The small diverticulum is positioned rostrolaterally just ventral to the corneoscleral junction. Light enters the diverticulum through an unpigmented ventrolaterally facing 'window' and, due to the disorganised orientation of the reflective crystals in the choroid and retinal tapetum medially, produces an unfocused image on the lateral diverticular retina; **(b)** *Winteria telescopa*. Due to the normally rostral orientation of the eye (not indicated here), the small diverticulum is located ventrolaterally and samples the caudolateral visual field. As in *O. soleatus*, illumination enters the diverticulum through an unpigmented area, allowing only unfocussed light perception; **(c)** *Macropinna microstoma*. The largest specimen sampled had a rostrolateral diverticulum covering around half of the lateral wall of the tube eye with a dorsal retina and a ventral cornea. Although our understanding of this diverticulum is incomplete, it seems unlikely that light entering the diverticulum produces a focussed image; **(d)** *Bathylychnops exilis*. The large rostrolateral diverticulum is characterised by a prominent, sclerally derived, lens. The light rays entering the diverticulum ventrolaterally are shown as focussed on the diverticula retina on the unproven assumption that the scleral lens is sufficiently refractive; **(e)** *Dolichopteryx longipes*. Ventrolateral illumination enters a large, laterally protruding, dorsal diverticulum through a cornea and impinges on the medial wall of the diverticulum, whose retinal-derived reflective plates change orientation throughout the diverticulum and produce a focussed image on a lateral retina (Wagner et al., 2009); **(f)** *Rhynchohyalus natalensis*. A large diverticulum covers the entire lateral wall of the tubular portion of the eye. Light entering the ventrolaterally directed diverticular cornea hits the medial wall whose choroidally derived reflective plates are all orientated approximately parallel to the surface and form an image on the lateral retina (Partridge et al., 2014). For those eyes in which a focussed image may be formed **(d–f)**, three entrant rays are shown converging to one point on the retina. For eyes in which the crystals in the RPE/choroid are disorganised, suggesting a more diffuse reflective surface **(a,b)**, only one entrant ray is shown with representative rays shown reflected at different angles.

of retinal ganglion cells in the main retina of *R. natalensis* is far lower than in *D. longipes* (**Table 2**), one might assume that the former will have a much-reduced potential spatial resolution. However, spatial resolution is also increased by a larger eye with a longer focal length. Consequently, eye size is positively correlated to spatial resolving power in many animals, including mesopelagic teleosts, and species with large eyes can have comparable spatial resolution to smaller species despite having lower ganglion cell densities (Collin et al., 1997; de Busserolles et al., 2014; Landgren et al., 2014). Thus, when the theoretical average resolving power of the main retina within the tubular portion of the eye is determined in *R. natalensis* and *D. longipes* as described by Collin and Pettigrew (1989), they are in fact very similar (1.35 and 1.28 cycles per degree, respectively), the larger eye of *R. natalensis* compensating for its low density of retinal ganglion cells. These spatial resolving powers are much lower than those cited for other mesopelagic teleosts (1.6–22.9 cycles per degree; Collin and Partridge, 1996; Collin et al., 1997, 1998; Wagner et al., 1998; Uemura et al., 2000; Landgren et al., 2014; de Busserolles et al., 2014). This is because in all animals, including mesopelagic teleosts with both tubular and more lateral eyes, the distribution of ganglion cells is not uniform within the retina. As the spatial resolving power of an animal is determined by the maximum ganglion cell density, the spatial resolution determined here using average cell densities will inevitably be significantly lower than those determined using maximum ganglion cell density in other studies.

An eye with a complex, potentially refractive, diverticulum (*Bathylychnops exilis*)

The structure of the *B. exilis* eye has been previously described (Pearcy et al., 1965; Munk, 1966) and in many respects our observations support the previous findings. Thus, in all animals examined to date, both here and elsewhere, the eye consists of a roughly hemispherical main globe whose retina is linked to that lining a well-developed diverticulum containing a sclerally derived lens covered internally by an unpigmented double ciliary epithelium. However, our interpretation of the eye of *B. exilis* differs in some important respects from that of previous studies.

For example, although the eye of *B. exilis* is not tubular, unlike previous authors, we found that the retina of the main eye, like more conventional tube eyes (**Supplementary Material 1**), has a well-developed main retina ventrally (**Figure 5f**) and a simpler 'accessory' retina on its vertical surfaces (**Figure 5g**). This, and the dorsal positioning of the lens, suggests that the main eye of *B. exilis*, although not overtly tubular, is related to such eyes. We also depart from the earlier studies in another respect. A structure so far unique to the eye of *B. exilis* is the prominent swelling in the sclera we observed caudal to the diverticulum (**Figure 5b**) in our specimen (SL 200 mm). Two similar swellings were also noted by previous authors in a larger animal (SL 470 mm) although they were absent entirely in smaller animals (SL 107 and 110 mm) (Pearcy et al., 1965; Munk, 1966), suggesting their presence is size/age dependant. Previous authors called these scleral swellings 'corneal projections,' thus implying an optical function. It was thought they might increase the visual field of the main eye by acting as additional lenses (Pearcy et al., 1965), a suggestion seemingly supported by their fine structure that closely resembles that of the scleral lens of the diverticulum. However, while the inner surface of diverticular scleral lens is covered by an unpigmented ciliary epithelium (**Figures 6a–c**), which allows light traversing the lens to reach the diverticular retina, the corneal projections are unlikely to bring additional light to the retina of either the main eye or the diverticulum as their inner surface is adjacent to the choroid and ciliary epithelium of the main globe, both of which contain dense aggregations of melanosomes (**Figures 6h,i**).

An obvious question regarding the *B. exilis* diverticulum is whether the scleral lens produces a focussed image on the diverticular retina. An important aspect to answering this question is the shape of the scleral lens. While Pearcy et al. (1965) state that it is spherical and Munk (1966) schematically represents it as such, the micrograph shown in Pearcy et al. (1965) suggests that the diverticular lens is in fact aspherical. In our sections it is, similarly, aspheric, being approximately hemispherical external to the diverticulum and internally semi-elliptical. Assuming no distortions due to preservation or sectioning, the optical properties of such a lens could be estimated but would be subject to many approximations. Another consideration is the location of the retina relative to the lens. In **Figure 5c**, the outline of the diverticulum is best shown by the sclera, the shape of which is likely to be relatively little affected by fixation. Laterally the diverticular retina has become detached from the sclera and is thus artifactually displaced inwards. Dorsally, however, it still appears in its normal position immediately adjacent to the sclera.

Without ray-tracing or direct observation, it is impossible to be certain about the optics of the *B. exilis* diverticulum. Nevertheless, selection pressure on eyes for the evolution of functional optics is generally strong and their evolution can be very rapid (Nilsson and Pelger, 1994). Superficially, the biconvex cross section of the diverticular lens suggests it acts as a refracting element, as long as its refractive index (RI) exceeds that of the surrounding seawater and intraocular media (both likely to be ca. 1.33). The RI of hydrated collagen, the main component of the sclera from which the diverticular lens is derived, is indeed somewhat higher than 1.33 (Sivak and Mandelman, 1982; Wang et al., 1996; Bashkatov et al., 2000). This might be further elevated by the inclusion of other substances, but we have no direct evidence of these, nor their distribution within the diverticular lens. The spherical lens constructed of lens fibres found in the non-diverticular eyes of most fish has a RI graded from ca.1.37 at its edge

to ca. 1.54 centrally (Fernald, 1990; Sivak, 1990; Jagger and Sands, 1996), producing a lens with low aberration and a low f-number (the ratio of focal length to lens aperture) of ca. 1.28. Assuming the position and shape of the scleral lens depicted in **Figure 5c** has not been affected by fixation or sectioning, and that it forms an image on the retina when light travels along its long axis, the scleral lens will have a focal length of ca. 2.67 mm, which with an aperture of 1.43 mm results in an f-number for distant objects of approximately 1.87.

In summary, although the diverticulum of *B. exilis* is potentially image forming (**Figure 10d**), its optical performance, and its functional ability to detect salient objects (i.e., relatively bright reflections or bioluminescent emissions) in the ventrolateral visual field, seen against a dark background, is yet to be determined.

The eyes of *Macropinna microstoma*

In a smaller specimen of *M. microstoma* (SL 32 mm) we observed a relatively simple rostrolateral diverticulum, similar to that of *O. soleatus* and *W. telescopa*, while the diverticulum of a larger animal (SL 55 mm) was more complex, larger and clearly visible externally and, most significantly, had a dome-shaped dorsally positioned retina (**Figures 8c–f**) and a ventral cornea. The only other description of the *M. microstoma* eye of two even larger animals (Frederiksen, 1973; SLs 119 and 125 mm), somewhat surprisingly, appear very similar to structures seen in our smallest animal.

Given our, possibly incomplete, current understanding of the diverticulum of the larger specimen of *M. microstoma,* it is impossible to say if it forms an image. As there is no lens in the diverticulum, any image formation would have to occur by reflection, most likely from the medial wall, as in *D. longipes* (Wagner et al., 2009) or *R. natalensis* (Partridge et al., 2014). While in the latter two species the diverticular retina is situated laterally and thus ideally positioned for image formation following reflection from a medial 'mirror,' in *M. microstoma* the retina is positioned dorsally and it is hard to imagine how this might lead to an effective image being formed in *M. microstoma*. However, as the two animals we sampled showed evidence of increasing diverticular size and complexity as fish grew larger, it is possible that had we sampled even larger animals they might indeed have an image forming diverticulum such as in *D. longipes* (Wagner et al., 2009) and *R. natalensis* (Partridge et al., 2014). Nonetheless, it seems likely that the diverticulum of the largest *M. microstoma* examined here serves only to detect unfocussed illumination entering through the ventral cornea and therefore examining visual space below the animal (**Figure 10c**). Although, as the eyes are mobile (Robison and Reisenbichler, 2008) they are, for example, sometimes directed rostrally in which case the caudal visual field would be sampled.

Effect of age/size on opisthoproctid ocular diverticular structure

As outlined above, different Opisthoproctidae have varying forms of diverticula, ranging from simple light detecting structures to more complex image-forming 'secondary eyes.' However, it may be unwise to assign a specific diverticular morphology to all individuals of a given species as, at least in some, the structure of a species' diverticulum changes during ontogeny.

It is likely that the extensive diverticula of larger *D. longipes*, *R. natalensis, B. exilis,* and *M. microstoma* develop from much smaller and simpler structures similar to those of *O. soleatus*, *W. telescopa* and *M. grimaldi*. Thus, while external examination (**Figures 3a,b** and **Supplementary Figures 2a,b**), histology (**Supplementary Figure 2c**) and MRI scans (**Figures 3c,g**) show that larger specimens of *D. longipes* (SLs 102 and 93 mm) have well-developed reflective diverticula protruding noticeably from the lateral wall of the tubular eye, MRIs of a smaller animal (SL 52 mm) (**Figures 3d,f,h**), show a reduced diverticulum which does not extend significantly from the lateral flank of the eye. Frederiksen (1973) also observed a protruding diverticulum in a large (SL 69 mm) *D. longipes* (although he did not appreciate its reflective optics), while Brauer (1908) described a much simpler, non-protruding diverticulum in the eyes of small (SL 35 mm) *D. anascopa*. Similar, small, diverticula were described in two other species of *Dolichopteryx* (Collin et al., 1997), although their specific identity and developmental status is uncertain.

Similarly, while an adult *R. natalensis* (SL 183 mm) had a complex reflective diverticulum occupying the entire lateral wall of the tube eye (**Supplementary Figures 3c–e**), it was much reduced in a postlarval animal (Bertelsen et al., 1965; Munk, 1966; SL 23 mm). The complex, dorsally directed, eyes of *B. exilis* with lensed rostroventral diverticula (**Figures 5a–c**; Pearcy et al., 1965; Munk, 1966) also develop from smaller, laterally positioned, eyes lacking an externally visible diverticulum (Stein and Bond, 1985; Badcock, 1988). Finally, although our description of *M. microstoma* is incomplete, it is clear that while the larger specimen examined here (SL 55 mm) had a well-developed protruding diverticulum (**Figures 8c–f**), the diverticulum of a smaller animal (SL 32 mm) was morphologically much less pronounced (**Figures 7a,d**).

The observation that the more complex diverticula in some species develop from simpler structures similar to the diverticula of *O. soleatus*, *M. grimaldi* and *W. telescopa* suggests an obvious question: Could the simple diverticula of the latter three species, develop into more complex structures in larger/older specimens? There is certainly need for caution. Although the sizes of the animals used by us and others to describe the simple diverticula of these animals are similar to those of animals routinely caught, these are not always representative of their recorded maximum sizes (**Table 1**). Fishing is a very selective technique for sampling deep-sea fauna, as the nets produce a lot of disturbance, stimulate bioluminescence and produce

acoustic noise, are generally towed very slowly (ca. 2 knots) and routinely have a relatively small mouth (typically 8 m^2). Experience shows that nets with bigger apertures (25 m^2–50 m^2) result in larger animals being caught. Therefore, most of the individuals captured are relatively small and it is possible larger, faster swimming, animals simply evade capture. Nonetheless, in the specimens of *O. soleatus*, *M. grimaldi,* and *W. telescopa* we and others have examined there have been no obvious signs of major ontogenetic change in their diverticula. We therefore feel it is unlikely that these animals develop more complex diverticula with age.

Eye movements and body position to change the visual field

The eyes of most teleosts with tubular eyes are normally orientated so that the main retina samples the dorsal visual field above the animal. Although this maximises sensitivity to dim downwelling sunlight and allows the binocular detection of dark silhouettes and bioluminescence above the animal, the visual field of the main retina is very restricted. A further problem may be that although the mouths of some species (e.g., *Argyropelecus* sp.), like the eyes, are upwardly directed, in most tube-eyed species the mouths are rostrally positioned and far from the eye's usual visual field, potentially making feeding problematic.

At least one opisthoproctid, *M. microstoma*, seems to have overcome these problems as the orientation of its tubular eyes is not, as was previously assumed, fixed. Observations of live *M. microstoma* both by a remotely operated vehicle (ROV) and in the laboratory showed that their normally dorsally orientated eyes can rotate rostrally towards the mouth (Robison and Reisenbichler, 2008). We suspect some other opisthoproctids may similarly be able to move their eyes.

For example, although the eyes of *D. longipes* are generally dorsally directed when animals are caught (**Supplementary Figure 2a**), in a freshly caught animal (**Figure 3b**), in our MRI scans (**Figures 3e,f**) and in some alcohol preserved museum specimens (HJW pers. obs.), their eyes are tilted rostrally to varying degrees, suggesting a degree of mobility. Brauer (1908) also observed two pairs of extraocular muscles, which he assumed were equivalent to the four rectus muscles of other vertebrates, in *D. anascopa*. Most convincingly, observations of a *D. longipes* filmed at 816 m depth south of El Hiero island (Canary Islands) from an ROV, clearly showed ocular motility (Ricardo Aguilar, Oceana[3]). Although the eyes of *R. natalensis* have not, as far as we know, been observed *in vivo*, the organisation of their extraocular muscles (Partridge et al., 2014) is similar to that of the mobile eyes of *M. microstoma* (Chapman, 1942), suggesting that they too may have mobile eyes.

Of interest are those species whose tubular eyes are not normally directed dorsally, but face rostrally towards the animal's mouth (*W. telescopa,* **Figures 2a–c,e**: *Stylephorus chordatus* and *Gigantura* sp.—Brauer, 1908; Munk, 1966; Locket, 1977; Collin et al., 1997). In *S. chordatus* and *Gigantura* sp., such eyes may nonetheless be directed towards the water surface, as these animals hang vertically in the water column (Pietsch, 1978; Robison and Reisenbichler, 2008; Kupchik et al., 2018), effectively 'standing on their tails.' Thus, their tube eyes are both directed at their mouths and towards the dim downwelling light and any bioluminescence above them, while their 'thread like' body minimises the animal's silhouette when seen from below. However, as *W. telescopa*, like *O. soleatus* produces bioluminescence from a rectal light organ (Bertelsen and Munk, 1964), which presumably acts to camouflage its ventral surface when seen from below (Denton et al., 1985; Haddock et al., 2010), it is unlikely that it normally adopts a similar vertical position in the water column and maintains a more 'normal' horizontal bodily orientation. Since this would mean its rostrally directed tubular eyes normally face forwards rather than upwards, seemingly depriving it of many of the benefits of tubular eyes, we suggest that the position of *W. telescopa* eyes may also not be fixed. Although, in preserved specimens their eyes invariably point rostrally, ocular orientation can be changed by applying only gentle mechanical pressure (RHD pers. obs.). Furthermore, a freshly caught specimen was seen to rotate its eyes from a rostral to a more dorsal position in the laboratory (NJM pers. obs.). Brauer (1908) also described four extraocular muscles in W. telescopa, although he regarded them as degenerate and doubted they could move the eyes significantly.

In this manuscript we have shown how the limited visual field of tube eyes can be extended by a variety of diverticula. The field of view of both the main and diverticular retinae may be further extended in some species by eye or even body movements. Consequently, the visual field of many opisthoproctids may not be as restricted as was initially assumed and large areas of visual space will not be left unattended.

Opisthoproctid phylogeny

The recovered phylogeny (**Figure 9**) is topographically similar to that of Poulsen et al. (2016), which relied entirely on mitogenomic data. It also includes three additional Opisthoproctidae (*W. telescopa*, *R. natalensis,* and *D. longipes*), whose eye structure has been described in detail, but that were not present in the Poulsen et al. (2016) phylogeny. Both phylogenies support the existence of a monophyletic group of short-bodied Opisthoproctidae relative to basal long-bodied species. They are also consistent with the presence

3 https://vimeo.com/592784545/91f2c7a6e8

of a monophyletic group of sole-bearing species within the short-bodied opisthoproctids. However, based on available data, it is not possible to fully resolve the relationships of non-soled, short-bodied species to one another, or to the soled species. Our phylogeny (**Figure 9**) is not time-calibrated, but Betancur et al. (2015) suggest that the divergence of the Opisthoproctidae (represented by *M. microstoma*) and the Argentinidae (represented by *Argentina silus* and *Glossanodon semifasciatus*) took place ca. 46Ma, which compares with the representation of the Opisthoproctidae (assigned to *Macropinna*) in the fossil record from Miocene deposits (7.24–13.82 Ma; Nazarkin, 2016).

The evolution of the most optically complex vertebrate eyes

In general, and specifically with regards to the eye, structurally and functionally simple organs become more complex as a result of further adaptation; however, morphological and molecular simplification can play a significant role in evolution (O'Malley et al., 2016). Some extreme examples of this phenomenon in the eyes of fish include the complete loss of eyes in blind cave fish (Krishnan and Rohner, 2017) and the degenerate eyes of some deep-sea fish, including the complete loss of optics in the bathy-demersal *Ipnops* sp. (Munk, 1966; Locket, 1977). Nonetheless, it is widely believed that, as suggested by Darwin (1859), the evolution of morphologically complex eyes was a multistep process involving a number of intermediate stages usually of increasing structural and functional complexity (Nilsson, 2021). A possible evolutionary sequence might be that simple non-directional dermal light-sensitive eye spots evolved into photoreceptors associated with screening pigment, providing rudimentary directional information. Such relatively simple structures in turn evolved into more complex eyes allowing at first low spatial resolution, and finally higher acuity vision such as that provided by 'human-type' eyes (Nilsson, 2021). Surprisingly, this whole sequence of events could have happened over relatively few generations, accounting for only a short period of evolutionary time (Nilsson and Pelger, 1994) and has occurred repeatedly and independently (Nilsson, 2021). The bipartite tubular eyes of opsithoproctids with image-forming lateral diverticula, often combining both reflective and refractive optics, are more anatomically and optically complex than most other vertebrate eyes. Could these, arguably the most complex of all vertebrate eyes, also have evolved from more 'normal' eyes by a similar step-by-step process?

Fish living in the photon-limited mesopelagic zone would likely benefit from any adaptation that increases absolute sensitivity, as long as the metabolic cost or constraints, such as those limiting body or eye size, allowed. For example, if a species would benefit from maximising sensitivity to the dim downwelling sunlight, individuals with eyes positioned more dorsally than the lateral, approximately spherical, eyes of most other vertebrates might gain a selective advantage. Additionally, individuals with large eyes may be favoured by selection as they can house large pupils, resulting in increased photon capture (Land and Nilsson, 2012), although the small size of most mesopelagic teleosts constrains the size of eye they can accommodate. Among mesopelagic myctophids, for example, eye size scales with standard length (de Busserolles et al., 2013). As most teleosts have a laterally compressed body, a teleost of a given size can accommodate a larger spherical eye if this is orientated laterally compared to dorsally. To avoid the loss of sensitivity associated with a reduction in eye size resulting from a dorsal positioning of the eyes, such eyes could be peripherally reduced maintaining only the central pupil, lens, and retina (**Figure 9** node B), which would allow the eye to have the same sensitivity as a larger spherical eye (Locket, 1977). The result of a gradual selection for dorsally positioned, peripherally reduced, eyes would be the upward-pointing tubular eyes of many mesopelagic fish. Such a gradual, stepwise, change in the position and shape of the eye is made credible by the fact that there are extant species with varying degrees of asymmetry between fully tubular dorsally positioned eyes and near spherical lateral ones (Munk, 1966; Locket, 1977; Marshall, 1979).

Although dorsally directed tubular eyes maximise absolute sensitivity, they have a very restricted visual field to which the Opisthoproctidae have adapted by evolving lateral or rostrolateral diverticula of varying complexity. These might also have evolved from a regular tubular eye *via* an incrementally beneficial series of steps. Initially, a simple mutation may have led to a loss of pigmentation to form a 'window' in the lateral wall of the tube eye. Since this wall is covered by a non-photosensitive ciliary epithelium (**Supplementary Figure 1a**), it is possible the lateral illumination entering the eye *via* the 'window' would have stimulated the accessory retina covering the medial wall of the tube. Although, the sensitivity to such illumination would be low, given the poorly developed nature of the accessory retina and the fact that the already dim light must traverse the eye in the absence of any optics, it might still be of benefit to the animal as it allows the perception of some lateral illumination. Sensitivity would be improved if the photosensitive tissue were positioned directly adjacent to the 'window.' This might arise *de novo* from the lateral ciliary epithelium which shares a common embryonic origin with the retina and has the potential to generate retinal neurons (Lamba and Reh, 2008; Demontis et al., 2012) and contains components of the phototransduction cascade in some species (Ghosh et al., 2004). Alternatively, photosensitivity near the unpigmented 'window' might arise from the adjacent accessory retina covering parts of the caudal or rostral walls of the tube. Sensitivity of this area would be further improved by

it being partially closed off medially by the intrusion of the reflective outer layers of the eye so that light not absorbed by the lateral photoreceptors could be reflected back onto them rather than lost within the body of the tube eye. The resulting structure would resemble the rudimentary diverticula, of *O. soleatus*, *M. grimaldi,* and *W. telescopa* and would allow simple lateral light detection. These relatively simple structures might then enlarge in some animals, *via* large but not image-forming diverticula of the type seen in *M. microstoma*, to result eventually in complex image-forming diverticula, as found in *B. exilis*, *D. longipes,* and *R. natalensis*. Each increase in complexity would result in increased sensitivity and would therefore be selected for.

Although the scenario described above for the evolution of dorsally positioned tubular eyes with variously developed diverticula may be superficially plausible, it lacks any direct evidence. It is also just one of several possible evolutionary sequences. Nevertheless, it is possible to consider the evolutionary changes from an ontogenetic perspective. Although the original view expressed by Haeckel that 'ontogeny recapitulates phylogeny' is largely discredited in such a simple form, an animal's development can have a similar path to its phylogeny. Notable examples are the ocular asymmetry of adult flatfish (Friedman, 2008) and the loss of eyes in troglobite cavefish (Krishnan and Rohner, 2017). Similarly, fish with tubular eyes begin life with 'normal' spherical, laterally placed, eyes (Brauer, 1902; Contino, 1939; Okamoto et al., 2004). Furthermore, as we have shown above, tube-eyed opisthoproctids with complex, laterally protruding, potentially image-forming diverticula, such as *D. longipes*, *R. natalensis,* and *B. exilis*, have more rudimentary, non-protruding light-sensing, diverticula earlier in their ontogeny. Thus, the developmental progression within individual species approximates the predicted evolutionary sequence.

A powerful indication of a possible evolutionary sequence of ocular traits is provided by phylogeny. In our phylogeny (**Figure 9**) the Argentiniformes comprise three families apart from the Opisthoproctidae; Argentinidae (e.g., *A. silus*, *G. semifasciatus*), Bathylagidae (e.g., *Lipolagus ochotensis*), and Microstomatidae (e.g., *Nansenia ardesica*). As the non-opisthoproctid argentiniform families do not have tubular eyes, it is likely that the common ancestor of all Argentiniformes (**Figure 9**, node A) had the roughly spherical, laterally positioned, eyes common to most vertebrates, which have been retained in all extant Argentiniformes that are not Opistoproctidae. The common ancestor of all Opisthoproctidae (**Figure 9**, node B), on the other hand, most likely will have had a simple tubular eye and may also have had a rudimentary, light-sensing, lateral diverticulum. The common ancestors of all short bodied opisthoproctids (**Figure 9**, node C) retained this ocular morphology as have all extant sole-bearing opisthoproctids, so far examined (*O. soleatus* and *M. grimaldi*).

One of the non-soled short bodied Opisthoproctidae, *W. telescopa*, also retained a simple diverticulum, which concurs with the view that the overall morphology of this genus is morphologically closest to the common ancestor of all opisthoproctids (Prokofiev, 2020). The other non-soled short-bodied opisthoproctids (*M. microstoma* and *R. natalensis*) developed more complex diverticula that, at least in the case of *R. natalensis*, form images by reflection.

In the two long-bodied opisthoproctids whose ocular morphology was studied here (*D. longipes* and *B. exilis*), the rudimentary diverticula of the common opisthoproctid ancestor have also evolved into larger, more complex ones that in *D. longipes* form images by reflection. Interestingly, *Bathylychnops* appears at a basal position within the Opisthoproctidae clade, comprising an independent lineage relative to the other genera (Prokofiev, 2020) and it is the only opisthoproctid whose diverticulum potentially produces images using refraction.

Interestingly, *R. natalensis*, whose diverticulum forms a focussed image by reflection, is more closely related to *W. telescopa*, and *M. microstoma* whose diverticula most likely do not form images, than to *D. longipes*, which also has an image-forming reflective diverticulum. If the presence of an image forming diverticulum alone would be a trait that has evolved only once in the Opisthoproctidae, then one might expect *R. natalensis* and *D. longipes* to be phylogenetically most closely related. However, the image-forming mirrors in the medial diverticular wall of *R. natalensis* and *D. longipes* are not only optically different, in the former image formation depends on the shape of the mirror's surface while the latter acts as a Fresnel-type reflector, but also have different origins: in *D. longipes* (Wagner et al., 2009) the reflective surface is derived from the retinal tapetum, while in *R. natalensis* (Partridge et al., 2014) it arises from the choroid. Thus, it appears that image forming diverticula have evolved on multiple occasions in this group. Interestingly, *W. telescopa* and *M. microstoma,* like *R. natalensis* have reflective crystals in the medial walls of their diverticula that are also derived from the choroid, which is consistent with their phylogenetic proximity.

The eyes of three genera of long-bodied opisthoproctid (*Bathylychnops*, *Duolentops*, *Ioichthys*) are not tubular when examined externally and have been described as pouch-like or vesicular (Prokofiev, 2020). Therefore, based on a superficial examination of morphology alone it may appear unlikely that the eyes of *B. exilis* originated from an ancestor with simple tubular eyes as suggested above. However, the main eye of *B. exilis* does have some of the features characteristic of tubular eyes (section **Supplementary Material 1**). For example, its lens and cornea are dorsally positioned, and its retina is clearly partitioned into a well-developed ventral main retina and a simpler 'accessory' retina lining the vertical walls of the eye (**Figure 5c**), an arrangement that is usually only found in tubular eyes. The more spherical eyes of *B. exilis* might therefore derive from classically tubular eyes. It is not unusual for evolution to favour simplified functional morphology as selective pressures change (Collin and Miglietta, 2008).

Collectively, both ontogenetic development and phylogeny are consistent with a gradual evolutionary pathway, in which tubular eyes with complex image-forming diverticula could have evolved from conventional laterally positioned eyes *via* a series of intermediate steps. What is noteworthy is that among the Opisthoproctidae different forms of complex diverticula have arisen on multiple occasions. Why this particular family of teleosts should boast such a diverse range of ocular morphologies remains an intriguing question. Further work studying the timing and ecological correlates of the ocular diversification of the Opisthoproctidae may provide some additional insight into the evolutionary processes. Moreover, this could be informed by clearer resolution of phylogenetic relationships using genome-scale data, and more detailed exploration of eye development from both morphological and transcriptomic data. Furthermore, a potentially powerful approach to understanding the diversity of ocular adaptations seen in the Opisthoproctidae would be to use the approaches of Nilsson and Pelger (1994) to identify the advantages of hypothetical intermediate anatomical structures between those seen today in living species and those inferred in ancestral species and the key selective pressures that may have led to this diversity.

Data availability statement

The data and code supporting the phylogenetic analysis are available at: doi: 10.5281/zenodo.7012696. All additional raw data supporting the conclusions of this manuscript will be made available by the authors on request.

Ethics statement

The MRI procedures were performed under University of Queensland Animal Ethics permit number: QBI/304/16. The histological work complied with the ethical guidelines of the University of Tübingen.

Author contributions

H-JW was responsible for planning and performing the histology which both H-JW and RD interpreted, while W-SC and NM performed the MRI. BR procured samples of *M. microstoma*. MG performed all phylogenetic analyses. JP, RD, H-JW, BR, and NM participated in the research cruises which gathered material for this manuscript and made observations on live animals or fixed museum specimens. RD, JP, and H-JW wrote early drafts of the manuscript. All authors contributed to the published version.

Funding

We are grateful for financial support to the German Ministry of Education and Technology (BMBF, PTJ) in funding various cruises with FS *Sonne*. NM was funded by the Australian Research Council.

Acknowledgments

Many thanks to Ulrich Mattheus for his unfailing and expert technical support and the masters, crew and scientists aboard all the research vessels involved in collecting the samples for this study. We are obliged to James Maclaine and Oliver Crimmen of the Natural History Museum, London and Dr. Tammy Horton of the National Oceanography Centre in Southampton for allowing access to their fish collections. Ricardo Aguilar of Oceana Europe kindly allowed access to a video of a live *D. longipes* filmed from an ROV. We are also grateful to the following for use of their images; Dr. Edie Widder (**Figure 1a**), the Information and Technology Dissemination Division of the Monterey Bay Research Institute (**Figure 8a**), Dr. Tammy Frank (**Supplementary Figure 2a**), and Dr. Adrian Flynn (**Supplementary Figure 3a**). We are also indebted to the University of Queensland Centre for Advanced Imaging for assistance with MRI. Many thanks to Dr. Adrian Flynn for capture of *Rhynchohyalus natalensis* (all other specimens were caught by the authors).

Conflict of interest

The authors declare that the research was conducted in the absence of any commercial or financial relationships that could be construed as a potential conflict of interest.

Publisher's note

Supplementary material

The Supplementary Material for this article can be found online at: https://www.frontiersin.org/articles/10.3389/fevo.2022.1044565/full#supplementary-material

References

Badcock, J. (1988). Evidence for the assignment of Dolichopteryx brachyrhynchus Parr to the genus *Bathylychnops* Cohen (Pisces. Opisthoproctidae). *J. Fish. Biol.* 32, 423–432. doi: 10.1111/j.1095-8649.1988.tb05378.x

Bashkatov, A. N., Genina, E. A., Kochubey, V. I., and Tuchin, V. V. (2000). Estimation of wavelength dependence of refractive index of collagen fibers of scleral tissue. In Controlling Tissue Optical Properties: Applications in Clinical Study. *Int. Soc. Opt. Photonics* 4162, 265–268. doi: 10.1117/12.405952

Bertelsen, E., and Munk, O. (1964). Rectal light organs in the argentinoid fishes Opisthoproctus and Winteria. *Dana Report* 62, 1–17.

Bertelsen, E., Theisen, B., and Munk, O. (1965). On a postlarval specimen, anal light organ, and tubular eyes of the argentoid fish *Rhynchohyalus natalensis* (Glichrist and von Bonde). *Vidensk. Medd. Dansk Naturh. Foren.* 128, 357–371.

Betancur, -R. R., Ortí, G., and Pyron, R. A. (2015). Fossil-based comparative analyses reveal ancient marine ancestry erased by extinction in ray-finned fishes. *Ecol. Lett.* 18, 441–450. doi: 10.1111/ele.12423

Borstein, S. R., and O'Meara, B. C. (2018). AnnotationBustR: An R package to extract subsequences from GenBank annotations. *PeerJ* 6:e5179. doi: 10.7717/peerj.5179

Brauer, A. (1901). Über einige von der Valdivia-Expedition gesammelte Tiefseefische und ihre Augen. *Sitzungsberichte der Gesellschaft zur Beförderung der Gesamten Naturwissenschaften zu Marburg* 8, 115–130.

Brauer, A. (1902). Über den Bau der Augen einiger Tiefseefische. *Verh. Dtsch. Zool. Ges.* 12, 42–57.

Brauer, A. (1908). Die Tiefseefische. 2. Anatomischer Teil. Wiss. Ergebn. Dtsch. Tiefsee-Exped. *'Valdivia'* 15, 1–266.

Chapman, W. M. (1939). Eleven new species and three new genera of oceanic fishes collected by the International Fisheries Commission from the northeastern Pacific. *Proc. U.S. Natl. Mus.* 86, 501–542. doi: 10.5479/si.00963801.86-3062.501

Chapman, W. M. (1942). The osteology and relationship of the bathypelagic fish *Macropinna microstoma*, with notes on its visceral anatomy. *Ann. Mag. Nat. Hist.* 11, 272–304. doi: 10.1080/03745481.1942.9755482

Chung, W.-S., Kurniawan, N. D., and Marshall, N. J. (2020). Toward an MRI-based mesoscale connectome of the squid brain. *iScience* 23:100816. doi: 10.1016/j.isci.2019.100816

Cohen, D. M. (1958). Bathylychnops exilis, a new genus and species of argentinoid fish from the North Pacific. *Stanford Ichthyol. Bull.* 7, 47–52.

Collin, R., and Miglietta, M. P. (2008). Reversing opinions on Dollo's Law. *Trends Ecol. Evol.* 23, 602–609. doi: 10.1016/j.tree.2008.06.013

Collin, S. P., and Partridge, J. C. (1996). Retinal specializations in the eyes of deep-sea teleosts. *J. Fish Biol.* 49, 157–174. doi: 10.1111/j.1095-8649.1996.tb06073.x

Collin, S. P., and Pettigrew, J. D. (1989). Quantitative comparison of the limits on visual spatial resolution set by the ganglion cell layer in twelve species of reef teleosts. *Brain Behav. Evol.* 34, 184–192. doi: 10.1159/000116504

Collin, S. P., Hoskins, R. V., and Partridge, J. C. (1997). Tubular eyes of deep-sea fishes: A comparative study of retinal topography (part 1 of 2). *Brain Behav. Evol.* 50, 335–346. doi: 10.1159/000113345

Collin, S. P., Hoskins, R. V., and Partridge, J. C. (1998). Seven retinal specializations in the tubular eye of the deep-sea pearleye, *Scopelarchus michaelsarsi*: A case study in visual optimization. *Brain Behav. Evol.* 51, 291–314. doi: 10.1159/000006544

Contino, F. (1939). Das Auge des argyropelecus hemigymnus morphologie, bau, entwicklung und refraktion. *Graefes Arch. Clin. Exp. Ophthalmol.* 140, 390–441. doi: 10.1007/bf01853754

Darwin, C. (1859). *On the origin of species by means of natural selection*. London: Murray.

de Busserolles, F., Fitzpatrick, J. L., Paxton, J. R., Marshall, N. J., and Collin, S. P. (2013). Eye-size variability in deep-sea lanternfishes (Myctophidae): An ecological and phylogenetic study. *PLoS One* 8:e58519. doi: 10.1371/journal.pone.0058519

de Busserolles, F., Marshall, N. J., and Collin, S. P. (2014). Retinal ganglion cell distribution and spatial resolving power in deep-sea lanternfishes (Myctophidae). *Brain Behav. Evol.* 84, 262–276. doi: 10.1159/000365960

Demontis, G. C., Aruta, C., Comitato, A., De Marzo, A., and Marigo, V. (2012). Functional and molecular characterization of rod-like cells from retinal stem cells derived from the adult ciliary epithelium. *PLoS One* 7:e33338. doi: 10.1371/journal.pone.0033338

Denton, E. J., and Warren, F. J. (1957). The photosensitive pigments in the retinae of deep-sea fish. *J. Mar. Biol. Assoc. U.K.* 36, 651–662. doi: 10.1017/s0025315400025911

Denton, E. J., Herring, P. J., Widder, E. A., Latz, M. F., and Case, J. F. (1985). The roles of filters in the photophores of oceanic animals and their relation to vision in the oceanic environment. *Proc. R. Soc. B* 225, 63–97. doi: 10.1098/rspb.1985.0051

Fernald, R. D. (1990). "The optical system of fishes," in *The visual system of fish*, eds R. H. Douglas and M. B. A. Djamgoz (Dordrecht: Springer), 45–61. doi: 10.1007/978-94-009-0411-8_2

Franz, V. (1907). Bau des eulenauges und theorie des teleskopauges. *Biol. Zentralbl.* 27, 271–350. doi: 10.1007/BF00428041

Frederiksen, R. D. (1973). On the retinal diverticula in the tubular-eyes opishthoproctid deep-sea fishes *Macropinna microstoma* and Dolichopteryx longipes. *Vidensk. Meddr. Dansk Naturh. Foren.* 136, 233–244.

Fricke, R., Eschmeyer, W. N., and Van der Laan, R. (2021). *Eschmeyer's catalogue of fishes:Genera, species, references*. Available online at: http://researcharchive.calacademy.org/research/ichthyology/catalog/fishcatmain.asp (Accessed June 2, 2021)

Friedman, M. (2008). The evolutionary origin of flatfish asymmetry. *Nature* 454, 209–212. doi: 10.1038/nature07108

Froese, R., and Pauly, D. (2021). *FishBase. World Wide Web electronic publication*. Available online at: www.fishbase.org, version (08/2021) (Accessed April 11, 2022)

Frőhlich, E., and Wagner, H.-J. (1998). Development of multibank rod retinae in deep-sea fishes. *Vis. Neurosci.* 15, 477–483. doi: 10.1017/s095252389815304x

Ghosh, S., Salvador-Silva, M., and Coca-Prados, M. (2004). The bovine iris–ciliary epithelium expresses components of rod phototransduction. *Neurosci. Lett.* 370, 7–12. doi: 10.1016/j.neulet.2004.07.026

Gilchrist, J. D. F., and von Bonde, C. (1924). "Deep-sea fishes procured by the SS "Pickle"," in *Issue 7 of Fisheries and marine biological survey report no. 3 for the year 1922. Special report*, part 2, (Cape Town: Cape Times).

Haddock, S. H., Moline, M. A., and Case, J. F. (2010). Bioluminescence in the sea. *Ann. Rev. Marine Sci.* 2, 443–493. doi: 10.1146/annurev-marine-120308-081028

Herring, P. J. (1990). "Bioluminescent communication in the sea," in *Light and life in the sea*, eds P. J. Herring, A. K. Campbell, M. Whitfield, and L. Maddox (Cambridge: Cambridge University Press), 245–264.

Jagger, W. S., and Sands, P. J. (1996). A wide-angle gradient index optical model of the crystalline lens and eye of the rainbow trout. *Vision Res.* 36, 2623–2639. doi: 10.1016/0042-6989(95)00328-2

Johnsen, S., and Haddock, S. H. D. (2022). *Macropinna*. *Curr. Biol.* 32, R256–R257. doi: 10.1016/j.cub.2022.02.020

Kozlov, A. M., Darriba, D., Flouri, T., Morel, B., and Stamatakis, A. (2019). RAxML-NG: A fast, scalable and user-friendly tool for maximum likelihood phylogenetic inference. *Bioinformatics* 35, 4453–4455. doi: 10.1093/bioinformatics/btz305

Krishnan, J., and Rohner, N. (2017). Cavefish and the basis for eye loss. *Philos. Trans. R. Soc. Lond. B Biol. Sci.* 372:20150487. doi: 10.1098/rstb.2015.0487

Kupchik, M. J., Benfield, M. C., and Sutton, T. T. (2018). The first in situ encounter of *Gigantura chuni* (Giganturidae: Giganturoidei: Aulopiformes: Cyclosquamata: Teleostei), with a preliminary investigation of pair-bonding. *Copeia* 106, 641–645. doi: 10.1643/ce-18-034

Lamba, D., and Reh, T. A. (2008). "Regenerative medicine for diseases of the retina," in *Principles of regenerative medicine*, eds A. Atala, R. Lanza, J. A. Thomson, and R. M. Narem (Amsterdam: Elsevier), 418–436. doi: 10.1016/b978-012369410-2.50025-5

Land, M. F. (1972). The physics and biology of animal reflectors. *Prog. Biophys. Mol. Biol.* 24, 77–106. doi: 10.1016/0079-6107(72)90004-1

Land, M. F. (1980). "Optics and vision in invertebrates," in *Handbook of sensory physiology VII/6B*, ed. H. Autrum (Berlin: Springer Verlag), 472–592. doi: 10.1007/978-3-642-66907-1_4

Land, M. F. (2000). Eyes with mirror optics. *J. Opt. Pure Appl. Opt.* 2, R44–R50. doi: 10.1088/1464-4258/2/6/204

Land, M. F., and Nilsson, D. E. (2012). *Animal eyes*. Oxford: Oxford University Press.

Landgren, E., Fritsches, K., Brill, R., and Warrant, E. (2014). The visual ecology of a deep-sea fish, the escolar *Lepidocybium flavobrunneum* (Smith, 1843). *Philos. Trans. R. Soc. Lond. B Biol. Sci.* 369:20130039. doi: 10.1098/rstb.2013.0039

Lanfear, R., Frandsen, P. B., Wright, A. M., Senfeld, T., and Calcott, B. (2017). PartitionFinder 2: New methods for selecting partitioned models of evolution for molecular and morphological phylogenetic analyses. *Mol. Biol. Evol.* 34, 772–773. doi: 10.1093/molbev/msw260

Locket, N. A. (1971). Retinal anatomy in some scopelarchid deep-sea fishes. *Proc. Royal Soc. B* 178, 161–184. doi: 10.1098/rspb.1971.0059

Locket, N. A. (1977). "Adaptations to the deep-sea environment," in *Handbook of Sensory Physiology Vol. VII/5*, ed. F. Crescitelli (Berin: Springer-Verlag), 67–192. doi: 10.1007/978-3-642-66468-7_3

Locket, N. A. (1980). Variation of architecture with size in the multiple-bank retina of a deep-sea teleost. Chauliodus sloani. *Proc. Royal Soc. B* 208, 223–242. doi: 10.1098/rspb.1980.0050

Marshall, N. B. (1979). *Developments in Deep-sea Biology*. Poole: Blandford Press.

Munk, O. (1966). Ocular anatomy of some deep-sea teleosts. *Dan. Rep.* 70, 1–62.

Nazarkin, M. V. (2016). *Barreleye Macropinna* sp. (Argentiniformes, Opisthoproctidae) from the miocene of sakhalin island, russia. *J. Vertebr. Paleontol.* 36:e1187158. doi: 10.1080/02724634.2016.1187158

Nilsson, D. E. (2021). "eye evolution in animals," in *The senses: A comprehensive reference*, 2nd Edn, ed. B. Fritsch (New York, NY: Elsevier), 1. doi: 10.1016/B978-0-12-805408-6.00013-0

Nilsson, D. E., and Pelger, S. (1994). A pessimistic estimate of the time required for an eye to evolve. *Proc. R. Soc. B* 256, 53–58. doi: 10.1098/rspb.1994.0048

Nilsson, D. E., Warrant, E., and Johnsen, S. (2014). Computational visual ecology in the pelagic realm. *Philos. Trans. R. Soc. Lond. B Biol. Sci.* 369:20130038. doi: 10.1098/rstb.2013.0038

O'Malley, M. A., Wideman, J. G., and Ruiz-Trillo, I. (2016). Losing complexity: The role of simplification in macroevolution. *Trends Eco. Evol.* 31, 608–621. doi: 10.1016/j.tree.2016.04.004

Okamoto, M., Sugisaki, H., and Ida, H. (2004). Development and distribution of the early life stages of the long?n pearleye *Benthalbella linguidens* (Aulopiformes: Scopelarchidae) in the western North Paci?c. *Ichthyol. Res.* 51, 301–308. doi: 10.1007/s10228-004-0233-7

Parin, N. V., Belyanina, T. N., and Evseenko, S. A. (2009). Materials to the revision of the genus *Dolichopteryx* and closely related taxa (*Ioichthys, Bathylychnops*) with the separation of a new genus Dolichopteroides and description of three new species (fam. Opisthoproctidae). *J. Ichthyol.* 49, 839–851. doi: 10.1134/s0032945209100014

Partridge, J. C., Douglas, R. H., Marshall, N. J., Chung, W.-S., Jordan, T. M., and Wagner, H.-J. (2014). Reflecting optics in the diverticular eye of a deep-sea barreleye fish (*Rhynchohyalus natalensis*). *Proc. Royal Soc. B* 281:20133223. doi: 10.1098/rspb.2013.3223

Pearcy, W. G., Meyer, S. L., and Munk, O. (1965). A 'four-eyed'fish from the deep-sea: *Bathylychnops* exilis Cohen, 1958. *Nature* 207, 1260–1262. doi: 10.1038/2071260a0

Pietsch, T. W. (1978). The feeding mechanism of Stylephorus chordatus (Teleostei: Lampridiformes): Functional and ecological implications. *Copeia* 1978, 255–262. doi: 10.2307/1443560

Poulsen, J. Y., Sado, T., Hahn, C., Byrkjedal, I., Moku, M., and Miya, M. (2016). Preservation obscures pelagic deep-sea fish diversity: Doubling the number of sole-bearing opisthoproctids and resurrection of the genus Monacoa (Opisthoproctidae. Argentiniformes). *PloS One* 11:e0159762. doi: 10.1371/journal.pone.0159762

Prokofiev, A. M. (2020). Revision of the generic classification of "Long-Bodied" Opisthoproctids (Opisthoproctidae) with a description of new taxa and new finds. *J. Ichthyol.* 60, 689–715. doi: 10.1134/s0032945220050094

Richardson, K. C., Jarett, L., and Finke, E. H. (1960). Embedding in epoxy resins for ultrathin sectioning in electron microscopy. *Stain Technol.* 35, 313–323. doi: 10.3109/10520296009114754

Robison, B. H., and Reisenbichler, K. R. (2008). *Macropinna microstoma* and the paradox of its tubular eyes. *Copeia* 2008, 780–784. doi: 10.1643/cg-07-082

Sivak, J. G. (1990). "Optical variability of the fish lens," in *The visual system of fish*, eds R. H. Douglas and M. B. A. Djamgoz (Dordrecht: Springer), 63–80. doi: 10.1007/978-94-009-0411-8_3

Sivak, J. G., and Mandelman, T. (1982). Chromatic dispersion of the ocular media. *Vision Res.* 22, 997–1003. doi: 10.1016/0042-6989(82)90036-0

Stein, D. L., and Bond, C. E. (1985). Observations on the morphology, ecology, and behaviour of *Bathylychnops* exilis Cohen. *J. Fish Biol.* 27, 215–228. doi: 10.1111/j.1095-8649.1985.tb04022.x

Tournier, J. D., Smith, R., Raffelt, D., Tabbara, R., Dhollander, T., Pietsch, M., et al. (2019). MRtrix3: A fast, flexible and open software framework for medical image processing and visualisation. *Neuroimage* 202:116137. doi: 10.1016/j.neuroimage.2019.116137

Uemura, M., Somiya, H., Moku, M., and Kawaguchi, K. (2000). Temporal and mosaic distribution of large ganglion cells in the retina of a daggertooth aulopiform deep–sea fish (*Anotopterus pharao*). *Philos. Trans. R. Soc. Lond. B Biol. Sci.* 355, 1161–1166. doi: 10.1098/rstb.2000.0659

Vaidya, G., Lohman, D. J., and Meier, R. (2011). SequenceMatrix: Concatenation software for the fast assembly of multi-gene datasets with character set and codon information. *Cladistics* 27, 171–180. doi: 10.1111/j.1096-0031.2010.00329.x

Vaillant, L. L. (1888). *Expéditions scientifiques du "Travailleur" et du "Talisman" pendant les années 1880, 1881, 1882, 1883*. Paris: Masson, 1–406. doi: 10.5962/bhl.title.98313

Vogt, K. (1980). Die Spiegeloptik des Flusskrebsauges. *J. Comp. Physiol. A* 135, 1–19. doi: 10.1007/bf00660177

Wagner, H.-J., Douglas, R. H., Frank, T. M., Roberts, N. W., and Partridge, J. C. (2009). A novel vertebrate eye using both refractive and reflective optics. *Curr. Biol.* 19, 108–114. doi: 10.1016/j.cub.2008.11.061

Wagner, H.-J., Fröhlich, E., Negishi, K., and Collin, S. P. (1998). The eyes of deep-sea fish II. Functional morphology of the retina. *Prog. Retin. Eye Res.* 17, 637–685. doi: 10.1016/s1350-9462(98)00003-2

Wagner, H.-J., Partridge, J. C., and Douglas, R. H. (2019). Observations on the retina and 'optical fold' of a mesopelagic sabretooth fish, *Evermanella balbo*. *Cell Tissue Res.* 378, 411–425. doi: 10.1007/s00441-019-03060-4

Wang, X. J., Milner, T. E., Chang, M. C., and Nelson, J. S. (1996). Group refractive index measurement of dry and hydrated type I collagen films using optical low-coherence reflectometry. *J. Biomed. Opt.* 1, 212–216. doi: 10.1117/12.227699

Warrant, E. J., and Locket, N. A. (2004). Vision in the deep sea. *Biol. Rev.* 79, 671–712. doi: 10.1017/s1464793103006420

Weale, R. A. (1955). Binocular vision and deep-sea fish. *Nature* 175, 996–996. doi: 10.1038/175996a0

Widder, E. A. (1999). "Bioluminescence," in *Adaptive mechanisms in the ecology of vision*, eds S. N. Archer, M. B. A. Djamgoz, E. R. Loew, J. C. Partridge, and S. Vallerga (Dordrecht: Kluwer Academic Publishers), 555–581. doi: 10.1007/978-94-017-0619-3_19